Research Paper

Prognostic analysis of tumor mutation burden and immune infiltration in hepatocellular carcinoma based on TCGA data

Shaoqing Liu[1,2,*], Qianjie Tang[3,*], Jianwen Huang[2,*], Meixiao Zhan[2], Wei Zhao[2], Xiangyu Yang[2], Yong Li[2], Lige Qiu[2], Fujun Zhang[1], Ligong Lu[2,&], Xu He[2]

[1]Department of Minimally Invasive and Interventional Radiology, Sun Yat-Sen University Cancer Center, State Key Laboratory of Oncology in South China, Collaborative Innovation Center for Cancer Medicine, Guangzhou 510060, China
[2]Zhuhai Interventional Medical Center, Zhuhai Precision Medical Center, Zhuhai People's Hospital Affiliated with Jinan University, Jinan University, Zhuhai 519000, China
[3]Department of Pharmacy, Guangdong Women and Children Hospital, Guangzhou 511400, China
*Equal contribution

Correspondence to: Fujun Zhang, Ligong Lu, Xu He; **email:** zhangfj@sysucc.org.cn, luligong1969@126.com, https://orcid.org/0000-0002-7850-7640; hexu220@163.com, https://orcid.org/0000-0002-7565-5111
Keywords: hepatocellular carcinoma, tumor mutation burden, The Cancer Genome Atlas, immune infiltration
Received: September 24, 2020 **Accepted:** January 14, 2021 **Published:** April 4, 2021

ABSTRACT

In order to explore the prognosis of tumor mutation burden (TMB) and the relationship with tumor infiltrating immune cells in hepatocellular carcinoma (HCC), we downloaded somatic mutation data and transcriptome profiles of 376 HCC patients from The Cancer Genome Atlas (TCGA) cohort. We divided the samples into high-TMB and low-TMB groups. A higher TMB level indicated improved overall survival (OS) and was associated with early pathological stages. One hundred and nine differentially expressed genes (DEGs) were identified in HCC. Moreover, based on four hub TMB-related signatures, we constructed a TMB Prognostic model (TMBPM) that possessed good predictive value with area under curve (AUC) of 0.701. HCC patients with higher TMBPM scores showed worse OS outcomes (p < 0.0001). Moreover, DCs subsets not only revealed higher infiltrating abundance in the high-TMB group, but also correlated with worse OS and hazard risk for high-TMB patients in HCC. Meanwhile, CD8+ T cells and B cells were associated with improved survival outcomes. In sum, high TMB indicates good prognosis for HCC and promotes HCC immune infiltration. Hence, DCs and the four hub TMB-related signatures can be used for predicting the prognosis in HCC as supplements to TMB.

INTRODUCTION

Hepatocellular carcinoma (HCC) is the most common pathological subtype of liver cancer; it is the sixth most common type of cancer and the fourth leading cause of cancer-related death in the world [1–3]. Although the main treatment of early HCC is surgery, 50% of the patients are at an advanced stage at the time of diagnosis [4]. The 5-year overall survival (OS) rate for HCC is about 12.5% [3, 5]. Targeted therapy has improved the OS in HCC; however, the overall efficacy is unsatisfactory. The emergence of immuno-therapy has identified new therapeutic prospects for HCC [6], especially immune checkpoint inhibitors (ICIs), such as programmed death 1 (PD-1)/ programmed death ligand-1 (PD-L1) and cytotoxic T-lymphocyte associated antigen-4 (CTLA-4) [7, 8]. In recent clinical studies, both nivolumab and

pembrolizumab have exhibited better prognosis as second-line therapy in advanced HCC after sorafenib treatment [9, 10].

Although ICIs therapy has been shown to be effective in several types of malignancies [11–15], it has shown varying effects in various types of cancer, even in the same cancer patients [15]. Hence, the identification of accurate biomarkers is an urgent need for screening patients who can benefit from immunotherapy and to monitor the prognosis of immunotherapy. Recently, an increasing number of biomarkers have been identified for predicting the efficacy of immunotherapy, including DNA damage repair (DDR) [16], microsatellite instability (MSI) [17, 18], neoantigens [19], and HLA presentation of neoantigens against tumor [20–22]. TMB is a novel biomarker that is calculated as genetic variations per million bases of the encoded genome [23, 24]. Patients with a high TMB have a superior objective response rate (ORR) and prolonged OS [19, 25, 26] than those with a low TMB. ORR differences can be explained by TMB in about 55% types of tumor [20]; however, TMB is not a single biomarker for predicting the efficacy of immunotherapy that may be inconsistent with specific genetic mutations in high-TMB patients. For example, patients with EGFR mutations and ALK rearrangements (EGFR+/LK+), JAK1 mutations, or JAK2 mutations are associated with low response to immunotherapy [27–30]. Meanwhile patients with KRAS mutations (KRAS+) had a better ICIs response rate [27], and STK11 mutation was found to be the main factor for PD-1 inhibitor resistance in lung adenocarcinoma with KRAS+ [31]. Moreover, tumor microenvironment (TME) has been well identified as a molecular determinant in many cancers. TUMEH [32] found that T cell infiltration in TME is closely related to the efficacy of immunotherapy. Moreover, higher infiltrating abundance of CD8+ T cell and memory activated CD4+ T cell subsets revealed prolonged OS in the high-TMB group [33]. Therefore, combined information from TMB levels, gene mutations, and immune infiltration density can be used as a novel biomarker for predicting the efficacy of immunotherapy in HCC.

The prognostic role of TMB and the relationship between TMB and immune infiltration varied for different types of cancers [33, 34], and limited studies have focused on TMB with immune infiltration in HCC. Thus, we investigated the prognostic role of TMB and the potential association between immune infiltration and hub TMB-related signature in HCC, using TCGA HCC cohort and Gene Expression Omnibus (GEO) datasets. We found that high TMB was a good prognostic predictor for HCC, and that DCs and the four hub TMB-related signatures could also be used for predicting the prognosis in HCC.

RESULTS

Genome-wide mutation profiling in HCC

The somatic mutation data of 376 HCC patients were processed from the TCGA (https://tcga-data.nci.nih.gov/tcga/) database and their clinical information has been presented in Table 1. The mean age was 61 years; 122 (32.4%) women and 254 (59.5%) men were included. Utilizing maftools software, we classified these mutations into various groups and exhibited mutation groups in box plots using various colors in box plots (Figure 1). The most common type was missense mutation (Figure 1A); single nucleotide polymorphism occurred more frequently than deletion (DEL) or insertion (INS) (Figure 1B), and C>T transition was the most common form of single nucleotide variants (SNV) in HCC (Figure 1C). The mutation categories are shown in box plots (Figure 1E). The top 10 mutated genes were TP53 (28%), TTN (25%), CTNNB1 (24%), MUC16 (16%), ABL (11%), PCLO (11%), MUC4 (10%), RYR2 (10%), ABCA13 (9%), and APOB (9%) (Figure 1F, 1G).

TMB was related to overall survival and clinical stage

We calculated the number of TMB per million bases for 363 samples and classified them into high-TMB and low-TMB groups using the median value as the threshold (Supplementary Table 1). Kaplan–Meier survival indicated that higher TMB was associated with better OS ($p = 0.0004$) (Figure 2A). However, high TMB was not in accordance with better disease-free interval (DFI) in this research (Figure 2B). Moreover, we found that higher TMB was also associated with tumor stage ($p = 0.035$; Figure 2C), pathologic stage ($p = 0.020$; Figure 2D), and T stage ($p = 0.027$; Figure 2E). The TMB levels tended to decrease with tumor progression (Figure 2C–2E), and clinical research with a larger sample size is required to verify this result.

Analysis of differentially expressed genes between the 2 TMB groups

The heatmap and volcano plot visualized that 109 differentially expressed genes (DEGs) were identified with limma software with $|logFC| > 1.5$ and false discovery (FDR) < 0.05 (Figure 3A, 3B and Supplementary Table 2). The Gene Ontology (GO) enrichment analysis demonstrated that in molecular function group, these DEGs were mainly involved in extracellular matrix structural constituent, glycosaminoglycan binding, and extracellular matrix structural constituent conferring tensile strength. In the biological process group, extracellular structure

Table 1. Clinical data of 376 patients with hepatocellular carcinoma (HCC) from the cancer genome atlas (TCGA) cohort in this research.

Level	Overall
N	376
Age (median [IQR])	61.00 [51.00, 69.00]
Gender (%)	
female	122 (32.4)
male	254 (67.6)
Status (%)	
Alive	243 (64.6)
Dead	132 (35.1)
Not Reported	1 (0.3)
pathologic_T (%)	
T1	185 (49.5)
T2	94 (25.1)
T3	81 (21.7)
T4	13 (3.5)
TX	1 (0.3)
pathologic_N (%)	
N0	257 (68.5)
N1	4 (1.1)
NX	114 (30.4)
pathologic_M (%)	
M0	272 (72.3)
M1	4 (1.1)
MX	100 (26.6)
pathologic_stage (%)	
Stage I	175 (49.7)
Stage II	86 (24.4)
Stage III	86 (24.4)
Stage IV	5 (1.4)
tumor_stage (%)	
stage i	175 (46.5)
stage ii	86 (22.9)
stage iii	86 (22.9)
stage iv	5 (1.3)
Unknown	24 (6.4)

organization, extracellular matrix organization, and cell-substrate adhesion were enriched. In addition, in the cellular component, TMB-related DEGs were mainly involved in collagen-containing extracellular matrix, extracellular matrix, and extracellular matrix component (Figure 4A–4C and Supplementary Table 3). Thereafter, we conducted Kyoto Encyclopedia of Genes and Genomes (KEGG) pathway analysis and found that TMB-related signatures were involved in several pathways, including fat digestion and absorption, cholesterol metabolism, and peroxisome proliferators-activated receptor (PPAR) signaling pathway (Figure 3C and Table 2). We then selected the top gene set enrichment analysis (GSEA) results of TMB-related items, wherein dilated cardiomyopathy, ECM-receptor interaction, focal adhesion, oocyte meiosis and small cell lung cancer were associated with TMB levels (Figure 3D). Moreover, we obtained protein–protein

interaction (PPI) networks with the STRING tool, and 36 proteins were related (Figure 4D).

Constructing a risk scoring model with differentially expressed genes

Further, we identified 30 prognostic signatures associated with TMB using univariate Cox regression model from the above 109 DEGs (Supplementary Table 4). In addition, we used multivariate Cox analysis to select four independent risk signatures with $p < 0.05$ and acquired the coefficients ($ß_i$) of the respective signature (Figure 5A and Table 3). The selection process was visualized on a Venn plot (Figure 5A). Among these four TMB-related genes, we found that the lectin galactoside-binding soluble 3 (LGALS3)

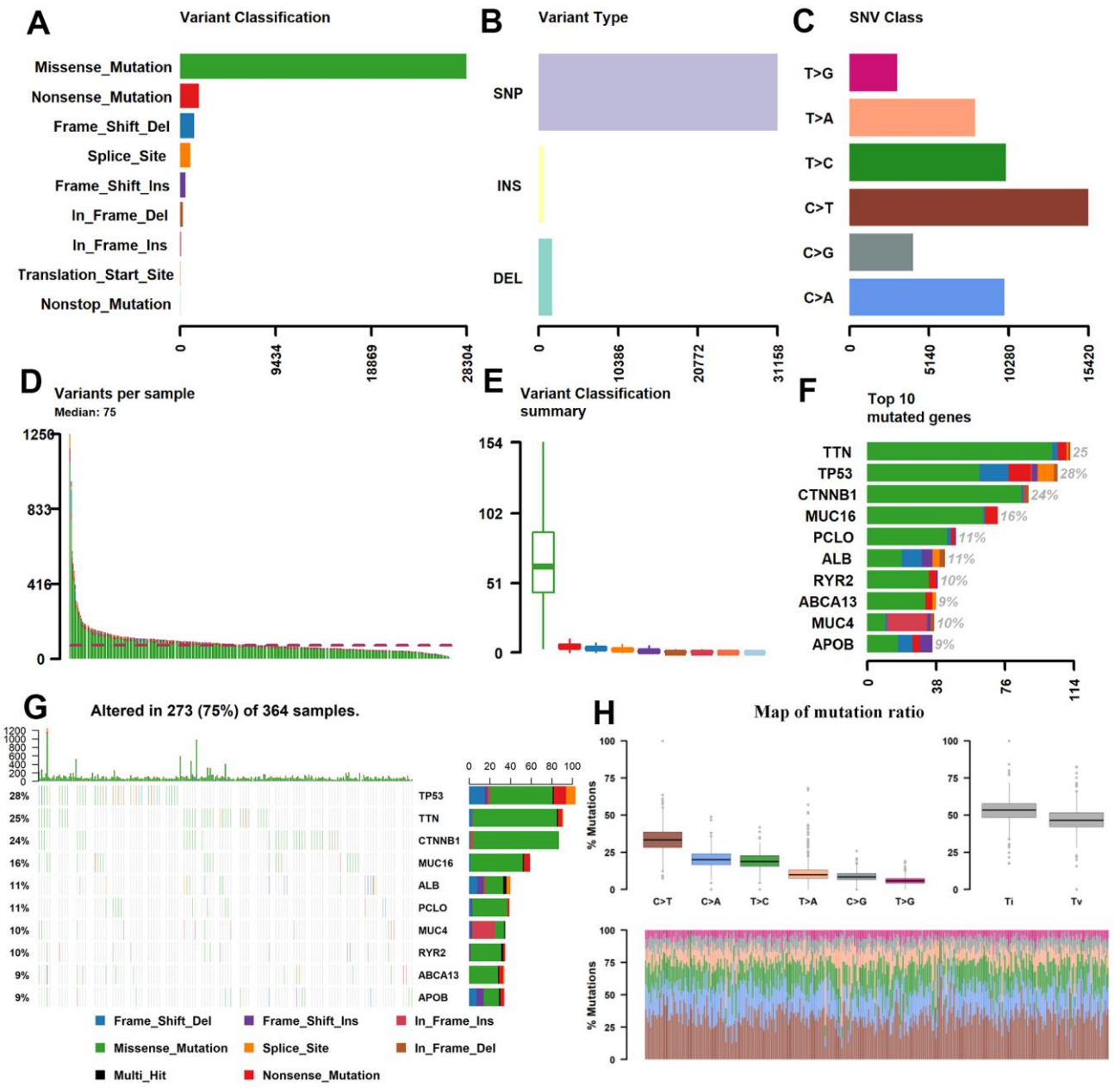

Figure 1. Statistics of mutation information in the HCC samples. (**A**–**C**, **H**) Statistical results of the different mutations, in which missense mutation occupied the most mutation classifications, SNP accounted for the main mutation type, and C>T was the main SNV Class. (**D**, **E**) Statistics of tumor mutations in each sample and different colors represent the different mutation types as shown in Figure 1A. (**F**) Statistics of different mutations in the top 10 hyper abrupt genes and different colors represent different mutation types. (**G**) The mutation status of the top 10 hyper abrupt genes: the X-axis is the sample, the Y-axis is the hyper abrupt gene, and different colors represent different mutation types. HCC, hepatocellular carcinoma; SNP, single nucleotide polymorphism; SNV, single nucleotide variants.

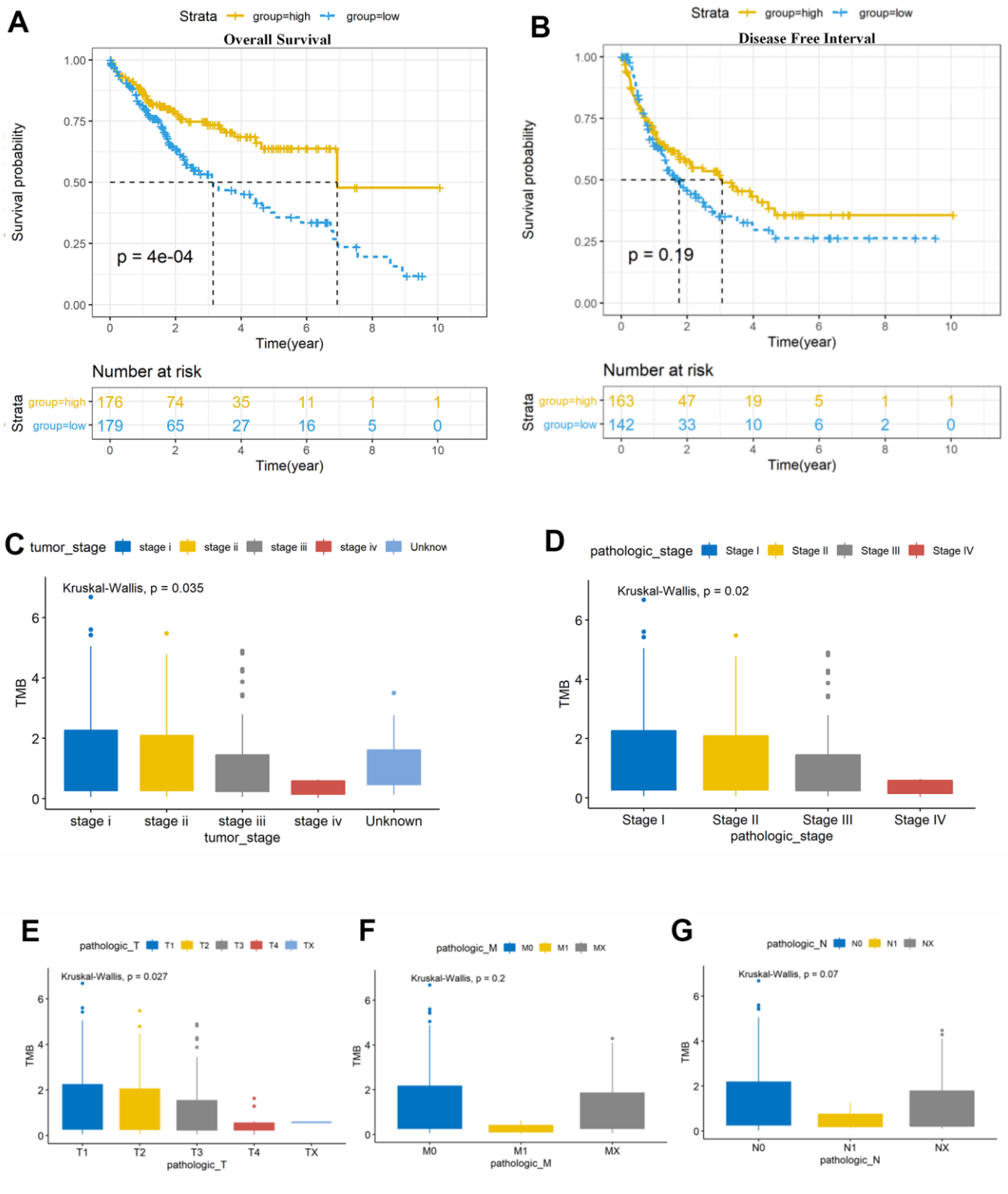

Figure 2. Prognosis analysis of tumor mutation burden (TMB) and correlation analysis with clinical risk features. (**A**) Patients with higher TMB had better overall survival (OS, P = 0.0014). (**B**) There was no association of TMB with disease-free survival (DFS, P = 0.51). (**C**, **D**) High TMB level was negatively correlated with tumor stage and pathological stage, with P = 0.035 and 0.02, respectively. Vertical and horizontal axes represent TMB value and different stages, respectively. (**E**–**G**) Significant difference was observed in the AJCC-T stages (P = 0.027), while no significant differences were observed in the AJCC-N and AJCC-M stages (P > 0.05). TMB, tumor mutation burden. Vertical and horizontal axes represent TMB value and different stages, respectively. TMB, tumor mutation burden; OS, overall survival; DFI, disease-free interval.

expression was upregulated in high-TMB groups than in low-TMB groups, and the expression of Nuclear Pore Complex Interacting Protein Family Member B15 (NPIPB15), Formimidoyltransferase Cyclodeaminase (FTCD), and Decorin (DCN) was negatively correlated with the TMB level (Figure 5B–5F). The hazard ratio (HR) with 95% confidence interval was shown in the forest plot (Figure 5G). Using the multivariate Cox regression model, TMBPM was constructed with the following formula: TMBPM = 0.179 x LGALS3 − 0.096 x NPIPB15 − 0.145 x FTCD − 0.126 x DCN. The multivariate model indicated that a high risk score was associated with poor survival (P < 0.001) (Figure 6A, 6B, 6D). Moreover, we classified the HCC patients into high-risk (n = 175) and low-risk (n = 175) groups using the median value as the cutoff value (Figure 6C, 6D). The receiver operating characteristic (ROC) curve for 5-year OS prediction suggested that the model possessed predictive accuracy with AUC = 0.701 (Figure 6C), and Kaplan–Meier plot showed that patients with high TMBPM revealed worse OS than those with low TMBPM (Figure 6D). Furthermore, HCC prognosis model nomograms were constructed based on different clinical characteristics (Figure 6E). We calibrated the 1-year, 3-year, and 5-year OS predictions for HCC patients, and all the calibrated curves were well-fitted

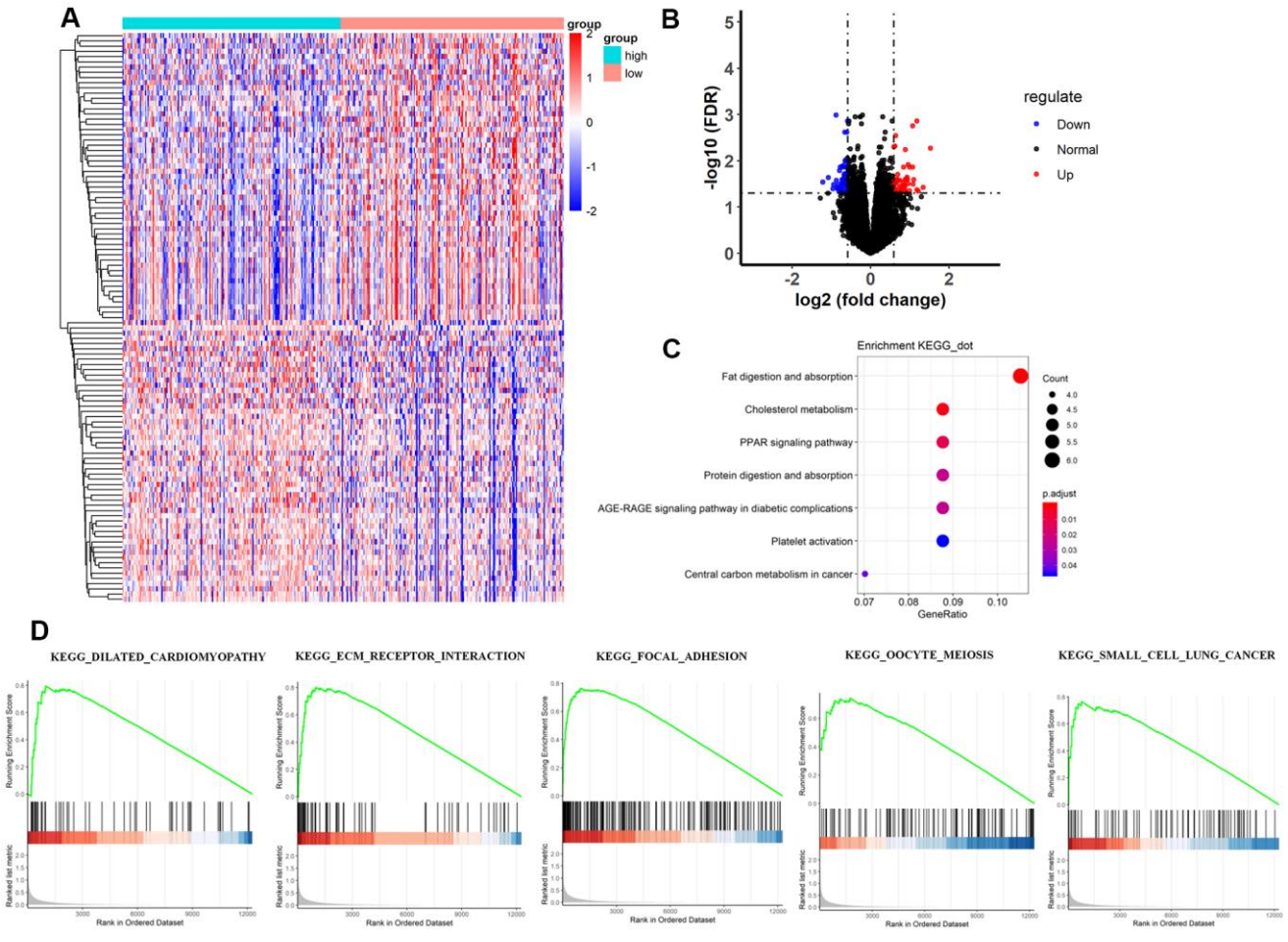

Figure 3. Comparisons of gene expression profiles in low-TMB and high-TMB groups and enrichment pathway analysis. (**A**) Top 109 DEGs are shown in the heatmap plot. Vertical and horizontal axes represent genes and HCC samples respectively, as ranked by TMB value. Genes with higher and lower levels are shown in red and blue, respectively. Color bars at the top of the heat map represent sample types, with pink and blue indicating low- and high-TMB samples, respectively. (**B**) Volcano plot of all DEGs were drawn with |log(FC) > 1| and FDR < 0.05. Each symbol represents a gene, and red, blue and black colors indicate upregulated, downregulated and normal genes, respectively. (**C**) KEGG pathway analysis revealed that these genes were involved in immune-related pathways, such as cholesterol metabolism; (**D**) Moreover, GSEA analysis shown that the top TMB-related crosstalk, including dilated cardiomyopathy, ECM-receptor interaction, focal adhesion, oocyte meiosis, and small cell lung cancer with FDR < 0.3. The vertical axis represents enrichment score. The enrichment score increased with the number of enriched genes and vice versa. DEGs, differentially expressed genes; TMB, tumor mutation burden; KEGG, Kyoto Encyclopedia of Genes and Genomes; ECM, extracellular matrix; HCC, hepatocellular carcinoma; GSEA, gene set enrichment analysis.

(Figure 6F–6H). Although TMBPM can accurately predict the 3-year and 5-year survival rate in HCC patients, whether the TMBPM maintained the independent predictive value needs to be investigated and validates on larger samples.

Comparison of immune cell abundance between high-TMB and low-TMB groups

Based on the newly developed CIBERSORT software [35], we intended to compare the differential profiles of immune fractions between the high-TMB and low-TMB groups. After filtering out patients with P > 0.05 with the "CIBERSORT" package, we obtained fractions of 22 immune cells in 56 HCC patients, and the results were displayed in the box (Figure 7A), where different colors represented various cell subsets.

Meanwhile, we revealed the differential abundance of immune cells between low-TMB and high-TMB groups with heatmap plot (Figure 7B), wherein we could intuitively find that CD8+ T cell, M0 macrophage, and M2 macrophage formed the majority of the components. Moreover, the Wilcoxon rank-sum test indicated that the infiltration levels of dendritic cells resting (P = 0.001), eosinophils (p < 0.001), and T cells regulatory (Tregs) (p = 0.02) were higher in the high-TMB group than in the low-TMB group (Figure 7C). In addition, the density of neutrophils (p = 0.006) showed a lower infiltrating level in the high-TMB group. In accordance with previous mutation analysis and Kaplan-Meier analysis, lower TMB commonly inhibited the immune infiltration levels in HCC patients, contrary to clear cell renal cell carcinoma (ccRCC) [36]. Macrophages were identified using CIBERSORT in HCC. Macrophages were significantly enriched in tumors and displayed similar proportions in the immune fractions of high- and low-TMB groups. Although M2 was a dominant Macophages, there were not clearly distinguished in M0, M1 and M2 macrophages, consistent with other previous reports [37, 38].

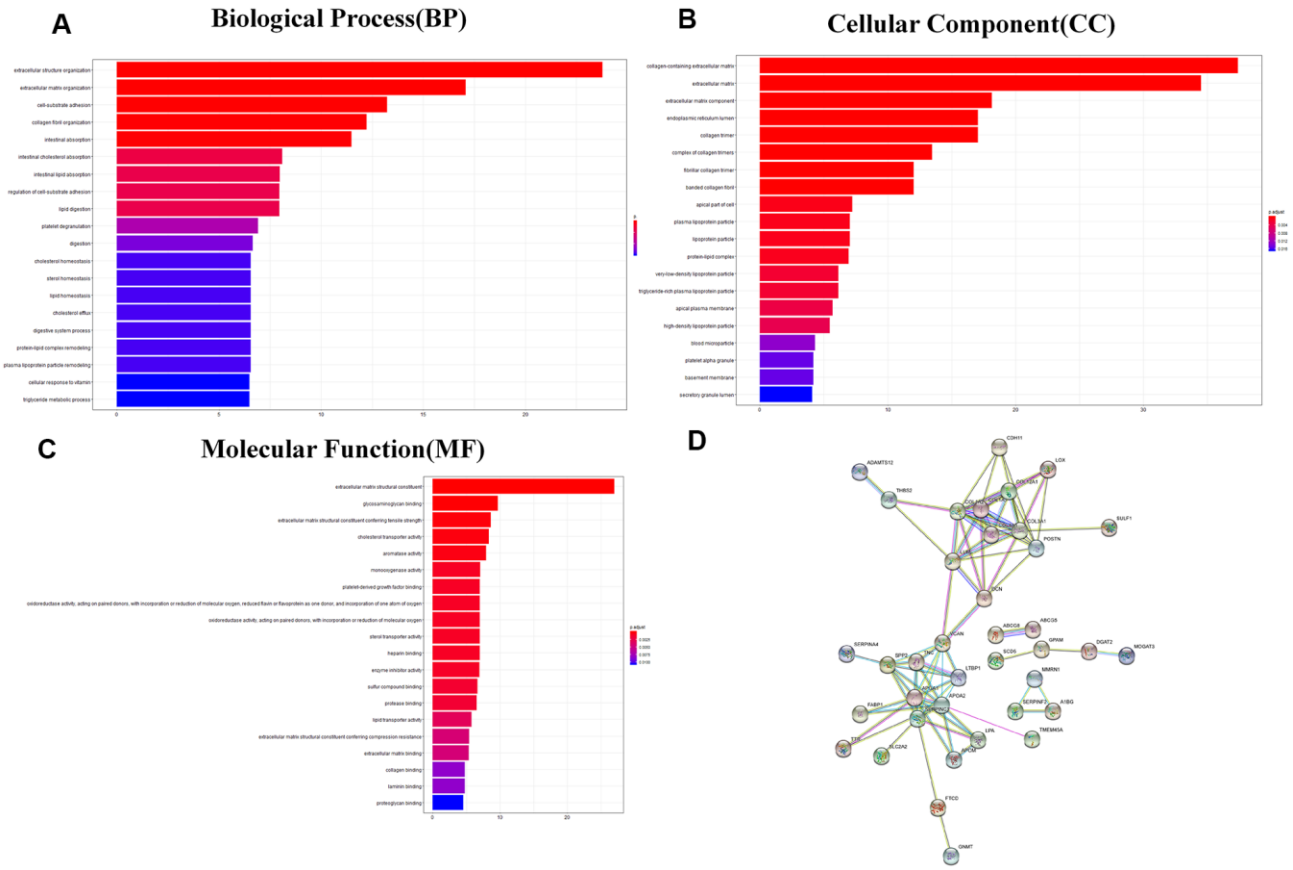

Figure 4. GO analysis and protein–protein interaction (PPI) analysis. (**A**–**C**) GO enriched results revealed that these DEGs were involved in the biological process, molecular function, and cellular component and other functional pathways. Metascape bar graph to view the top twenty non-redundant enrichment clusters. The enriched biological processes were ranked by p value. A deeper color indicates a smaller p-value. Vertical axes represent different pathway. (**D**) Thirty-six proteins were related in the protein–protein interaction. GO, Gene Ontology; PPI, protein–protein interaction; DEGs, differentially expressed genes.

Table 2. Kyoto encyclopedia of genes and genomes (KEGG) pathway analysis for the differential genes.

Description	Generatio	Pvalue	p.adjust	qvalue	geneID
Fat digestion and absorption	6/57	4.80E-07	8.45E-05	7.84E-05	ABCG5/DGAT2/MOGAT3/APOA1/FABP1/ABCG8
Cholesterol metabolism	5/57	2.48E-05	0.002180513	0.002021408	APOA2/ABCG5/LPA/APOA1/ABCG8
PPAR signaling pathway	5/57	0.000199794	0.011721233	0.010865975	APOA2/SCD5/ACSL6/APOA1/FABP1
Protein digestion and absorption	5/57	0.000531847	0.023401248	0.02169374	COL12A1/COL3A1/SLC7A9/COL1A2/COL1A1
AGE-RAGE signaling pathway in diabetic complications	5/57	0.000672758	0.023681078	0.021953152	NOX4/AKT3/COL3A1/COL1A2/COL1A1
Central carbon metabolism in cancer	4/57	0.001465681	0.042993318	0.039856246	AKT3/KIT/PFKP/SLC2A2
Platelet activation	5/57	0.001768727	0.044470846	0.041225963	AKT3/PRKG1/COL3A1/COL1A2/COL1A1
ECM-receptor interaction	4/57	0.003392436	0.074633591	0.069187838	TNC/COL1A2/COL1A1/THBS2

*KEGG, Kyoto Encyclopedia of Genes and Genomes; PPAR, peroxisome proliferators-activated receptor; ECM, extracellular matrix. GeneRatio: Annotation of genes in this pathway, annotation of genes in all KEGG pathways, and the ratio of the two; BgRatio: All genes annotated to pathway, all genes annotated to KEGG pathways, and the ratio of the two. Pvalue: P value of hypergeometric test; P.adjust: The P value corrected by multiple hypothesis testing; Qvalue: Q value; GeneID: geneID annotated to the pathway; Count: The number of genes annotated to the pathway.

We intended to compare the differential profiles of immune fractions between the high TMB and low TMB groups; therefore, we further intended to investigate the potential prognosis of immune cells based on the Tumor Immune Estimation Resource (TIMER) database. Multivariate Cox analysis showed that higher macrophage (HR = 29.333, P = 0.023), dendritic cells (HR = 21.823, P = 0.013) infiltrates comprised hazard factors with poor OS rates (Table 4 and Figure 8B, 8C), while the density of B cells (HR = 0.005, P = 0.040) or CD8+ T cell (HR = 0.021, P = 0.006) were marginally protective infiltrating cells (Table 4). Furthermore, the Kaplan–Meier analysis explained that higher infiltration levels of CD8+ T cells and B cells were associated with improved survival outcomes in HCC (Figure 8C).

Furthermore we investigate 28 subpopulations of immune cells based on the GSEA database (https://tcia.at/home) (Figure 9A and Table 5). The identified immune cells included T cells (activated T cells, central memory (Tcm), effector memory (Tem) CD4+ and CD8+ T cells, gamma delta T cells (Tγδ), regulatory T cells (Treg), follicular helper T cells (Tfh), T helper 1 (Th1), Th2, Th17), B cells (activated, immature, and memory B cells), myeloid-derived cells (macrophages, activated, plasmocytoid and immature dendritic cells (DCs), monocytes, mast cells, eosinophils, neutrophils,), NK, natural killer T cells (NKT), and MDSCs. All these cell subtypes were shared between the two-groups, albeit at different proportions (Figures 7C, 9A). The infiltration levels of B cells, tregs were relatively low in all patients, meanwhile the infiltration levels of DCs and the other T cells were higher in all patients (Figures 7C, 9A) consistent with a previous report [37]. Other immune cell types varied between high TMB and low TMB patients, revealing substantial heterogeneity of immune cell compositions among HCC tumors (Figures 7C, 9A).

DCs infiltrates in HCC indicated survival outcomes

The results of the cellular characterization of the immune infiltrates using GSEA showed that the infiltration of Tem CD8+ cells (HR = 0.754, p = 0.013), Tcm CD4+ cells (HR = 0.342, p = 0.011), Activated B cell (HR =0.821, p = 0.027), Memory B cell (HR =0.814, p = 0.044), Natural killer (NK) cell (HR = 0.732, p = 0.008) and Mast cell (HR = 0.612, p = 0.032) were associated with good prognosis, whereas activated CD8+ cells (HR = 2.415, p = 0.002), activated CD4+ cells (HR = 1.120, p = 0.008) and Tem CD4+ cells (HR = 2.612, p = 0.004) were associated with bad prognosis (Table 5). Although higher myeloid-derived suppressor cells (MDSCs) infiltration and lower Tregs infiltration associated with improved OS (Figure 8G, 8H), MDSCs (HR = 0.730, p = 0.307) and Tregs (HR = 0.966, p = 0.647) (Table 5) which are significantly associated with bad prognosis in other cancer [39] were not hazard risk (Table 5) for HCC in our study, and we also don't observed separation of the MDSCs and Tregs subpopulations related to immune suppression from the subpopulations related to the effector function (activated T cells, Tcm, Tem CD4+ and CD8+ cells) (Figure 9B, 9C). The separation was found in other cancers including lung squamous cell carcinoma, ovarian cancer, pancreatic cancer, and melanoma [39].

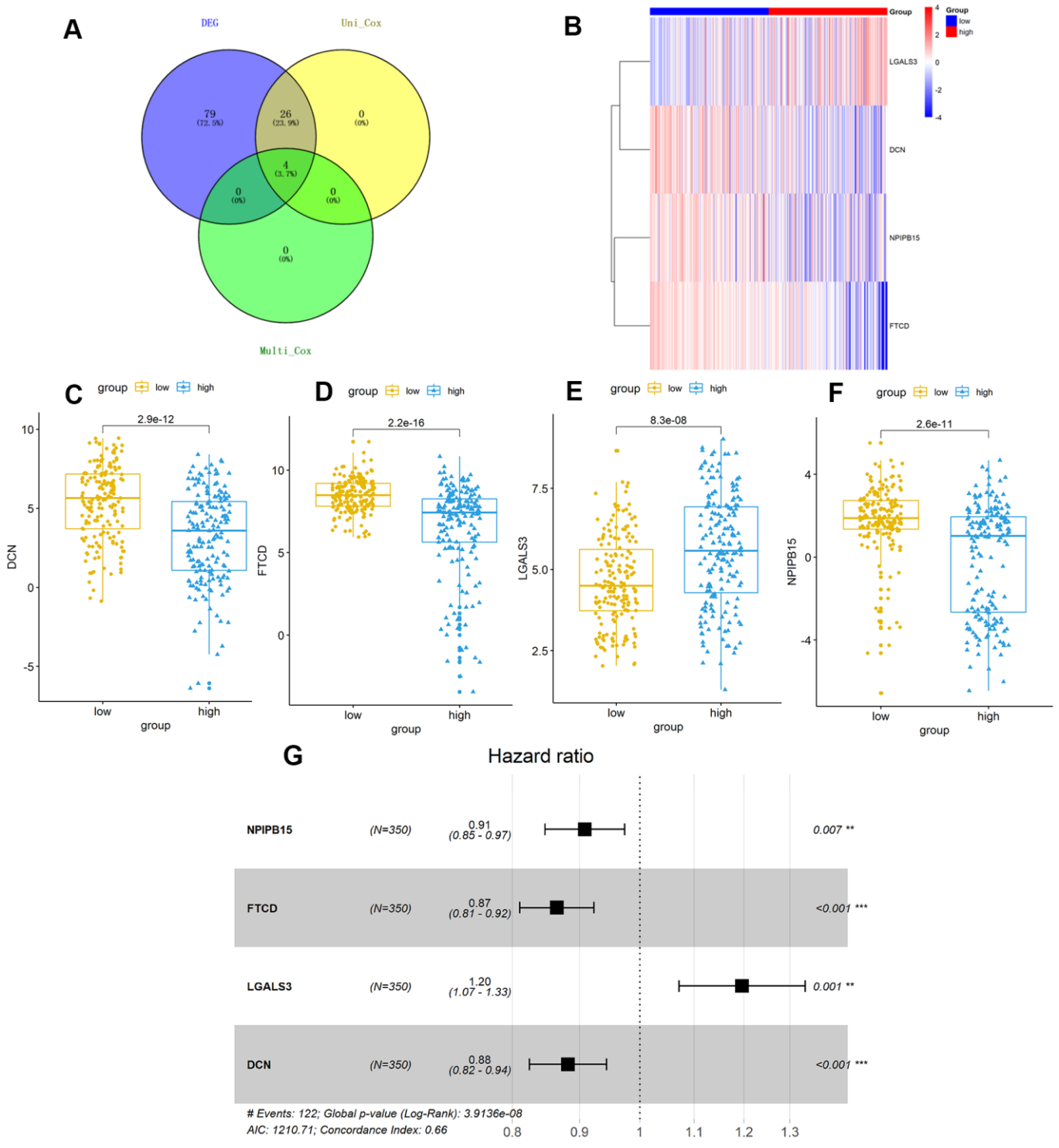

Figure 5. TMB-related hub-genes analysis. (**A**) Four TMB-related hub-genes were obtained with stepwise regression screening. (**B**) The four TMB-related hub-genes were shown in the heatmap plot. Vertical and horizontal axes represent TMB-related hub-genes and HCC samples respectively, as ranked by TMB value. Genes with higher and lower levels are shown in red and blue, respectively. Color bars at the top of the heat map represent sample types, with red and blue indicating high- and low-TMB samples, respectively. (**C**–**F**) LGALS3 (**E**) had higher expression in high-TMB group ($P < 0.01$), while DCN (**C**), FTCD (**D**), and NPIPB15 (**F**) were negatively correlated with high-TMB ($P < 0.01$). (**G**) Calculated by Cox multivariate model, hazard ratio with 95% confidence interval (95% CI) for each independent TMB-related signature are shown in forest plot. TMB, tumor mutation burden; HCC, hepatocellular carcinoma.

Table 3. Multivariate Cox analysis of TMB-related signature for HCC patients.

Var	Coef	HR	CI95.low	CI95.high	Zscore	P_value
NPIPB15	−0.096	0.908	0.847	0.974	−2.709	0.00675
FTCD	−0.145	0.865	0.811	0.923	−4.366	1.30E-05
LGALS3	0.179	1.196	1.071	1.335	3.18	0.001473
DCN	−0.126	0.882	0.824	0.943	−3.651	0.000261

*Var: Cox univariate analysis TMB-related genes; Coef: Risk coefficient; HR: relative risk value; Ci95.low, CI95.high: range of 95% confidence interval of relative risk value HR; Zscore: Z value of statistical test; P_value: the P value tested by Cox test with multi-factor; HCC: hepatocellular carcinoma; TMB: tumor mutation burden.

The progression was also characterized by distinct immune cell patterns between high-and low-TMB group based on GSEA database. Within each TMB group, the composition of the immune cells was divergent in HCC. For example, activated DCs, EOS and Neu were enriched in stage I and stage II tumors and only depleted in stage III in high-TMB patients (Figure 9D), and that activated CD4 and Mem_B were only depleted in late stage tumors and enriched in early stage tumors (Figure 9D) in low-TMB samples. There were not any pots in stage IV for high-TMB, because there were not enough samples for analysis (Figure 9D). Meanwhile, Univariate Cox analysis showed that higher levels of mDCs (HR = 21.823, P = 0.013) and Imm_DC (HR = 10.151, p = 0.022) with poor OS rates (Tables 4, 5 and Figure 8C, 8I) were hazard factors in High TMB group, while higher density of pDCs (HR = 0.302, p = 0.021) with improved OS rates (Figure 8J, P < 0.01) was marginally protective infiltrating cells in low-TMB groups. These results might explain why some patients with high TMB are not responsive to therapy with checkpoint blockers and also why some patients with low TMB are responders.

In summary, these analyses showed that both the genomic profiles and the specific tissue context contribute to the cellular composition of the immune infiltrates. Furthermore, whether using CIBERSORT, TIMER database or GSEA database, it is noteworthy that inflated levels of DCs and prognosis of DCs were different between high-TMB and low-TMB groups. mDCs and immature DCs subsets showing higher infiltrating abundance in the high TMB group was associated with lowered OS and higher risk factor, indicating that these high TMB HCC patients with higher infiltrates of mDCs and immature DCs had poor survival outcomes, meanwhile the higher fraction of pDCs was lower risk factor and was associated with better OS in low TMB samples. Accordingly, Kaplan–Meier analysis and Wilcoxon rank-sum test showed that dendritic cells can also be used as secondary prognosis indicators for immunotherapy in HCC.

DISCUSSION

Liver cancer (LC) remains the most common cause of cancer-related death and the second major cause of cancer-related death worldwide, despite considerable improvements in its treatment [2]. Since 2017, immune checkpoint inhibitors (ICIs) have showed promising results in the immunotherapy for advanced HCC [9]. However, few HCC patients are able to obtain benefits from this treatment. Thus, many researches have focused on the identification of predictive biomarkers for immunotherapy.

In the current research, we found that mutations in TP53 (28%), CTNNB1 (24%), and TTN (25%) are frequently found in HCC (Figure 1). Wang found that HCC patients with TP53 mutation were significantly correlated with high TMB (P = 0.0005) and exhibited poor prognosis (OS: HR = 1.58, P = 0.0109) [40], indicating that HCC patients with TP53 mutation were more likely to benefit from immune treatment. Furthermore, CTNNB1 mutation was positively correlated with TMB-H and TP53 in HCC [41]. A meta-analysis found that NSCLC patients with EGFR mutation could not benefit from immunotherapy, and EGFR-positive patients had low TMB [42, 43].

TMB is a novel prognosis biomarker for ICIs therapy in breast cancer [44] and other tumors [45, 46]. Robert found that high somatic TMB patients treated with ICIs exhibited better OS [45]. Hellmann demonstrated that small-cell lung cancer patients with high TMB treated with either nivolumab plus ipilimumab or nivolumab monotherapy had better prognosis, irrespective of the level of PD-L1 expression [25]. In this study (Figure 2), HCC patients with high TMB had significantly better OS (p = 0.0014) than those with other malignancies [33]; moreover, higher TMB may induce immune recognition and prognosis improvement. Further, TMB was negatively correlated with the tumor stages (P = 0.035) and AJCC-T stages (P = 0.027) (Figure 2E). These results suggest that the TMB level declined with

tumor invasion and progression; this prompted us to investigate the potential relationship among TMB, DEGs, and immune infiltrates for identifying more prognostic biomarkers for HCC.

Subsequently, four hub TMB-related signatures were identified (Figure 5 and Table 3) on univariate and multivariate Cox analysis (positive correlation: LGALS3, negative correlation: NPIPB15, FTCD and DCN). Furthermore, a prognostic model (TMBPM) was developed using four hub TMB-related signatures that can be very useful for survival prediction (Figure 6 and Table 3). To our knowledge, this is the first TMB prognostic model to predict survival outcomes in HCC.

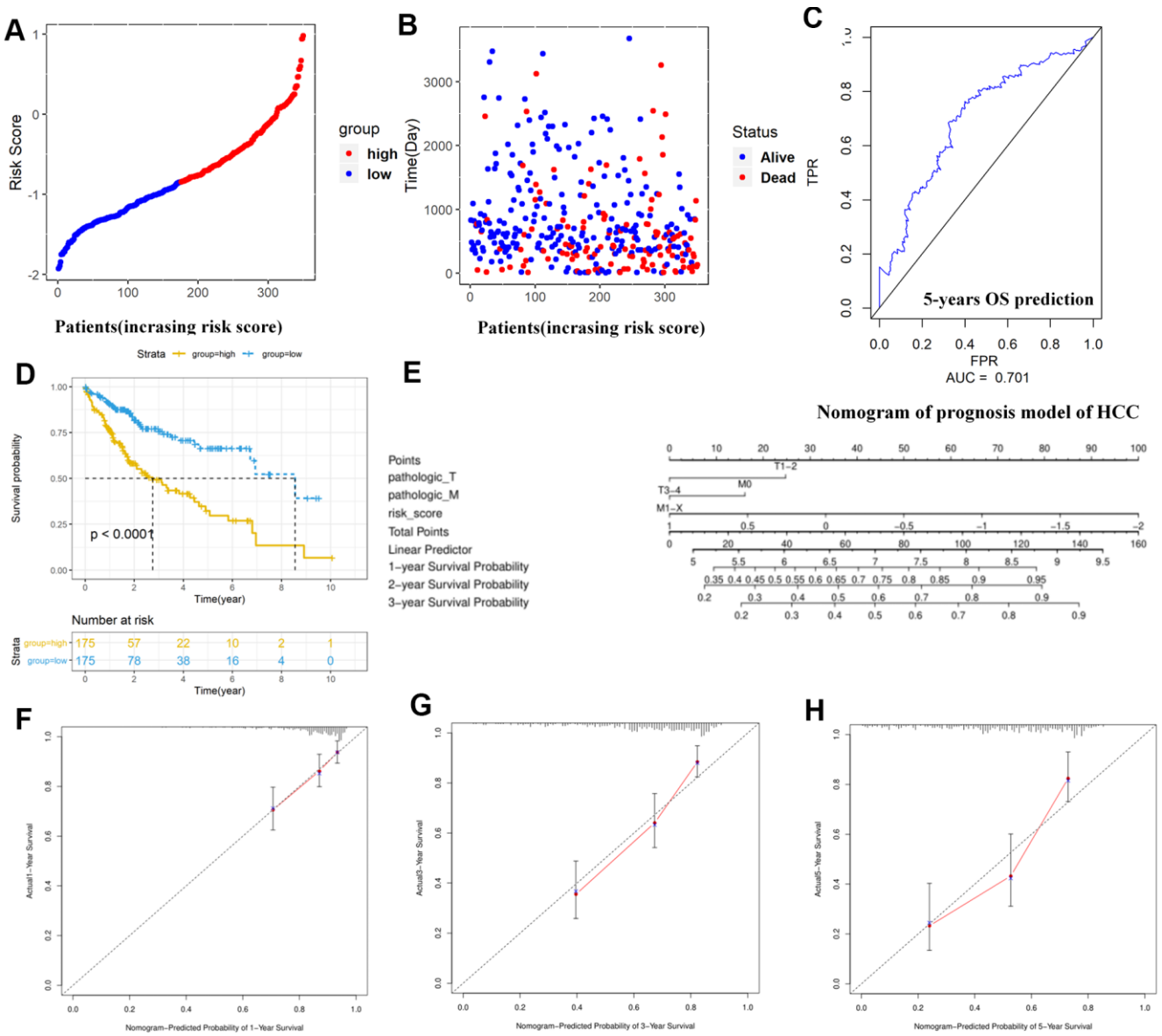

Figure 6. Construction and assessment of TMBPM for HCC. (**A**, **B**) Distribution of the risk score for each HCC patient as per the TMBPM levels. Vertical and horizontal axes respectively represent risk score and OS patients, as ranked by increasing risk score. Red and blue colors respectively represent high and low risk cases. (**B**) Dot plot of Survival time for each HCC patient as per the TMBPM levels. Vertical and horizontal axes respectively represent survival times and OS patients, as ranked by increasing risk score. Read and blue colors represent dead and living OS cases, respectively. (**C**) Horizontal and vertical axes are false positive rates and true positive rates, respectively. The AUC value of the ROC plot was 0.701 that showed superior predictive accuracy of TMBPM. (**D**) Kaplan-Meier analysis demonstrated that higher TMBPMs showed worse OS with P < 0.0001. (**E**) Nomogram of the prognosis model of HCC. (**F**–**H**) All the calibration curves of 1-year (**F**), 3-year (**G**), and 5-year (**H**) prognosis model fitted well. HCC, hepatocellular carcinoma; TMBPM, tumor mutation burden prognostic model; OS, overall survival; ROC, receiver operating characteristic; AUC, area under the curve; TPR, true positive rates; FPR, false positive rates.

Patients with a high TMBPM score had worse survival outcomes. Moreover, the AUC of the ROC curve was 0.701, indicating the prediction accuracy of the TMBPM. Although we calibrated the curves of 1-year, 3-year, and 5-year prognosis prediction models, further research on larger samples is needed before clinical application. In bladder cancer (BLCA) [33], tumor mutation burden related signature (TMBRS) mode were constructed by eight hub TMB-related signatures for prognosis prediction. Although this method can

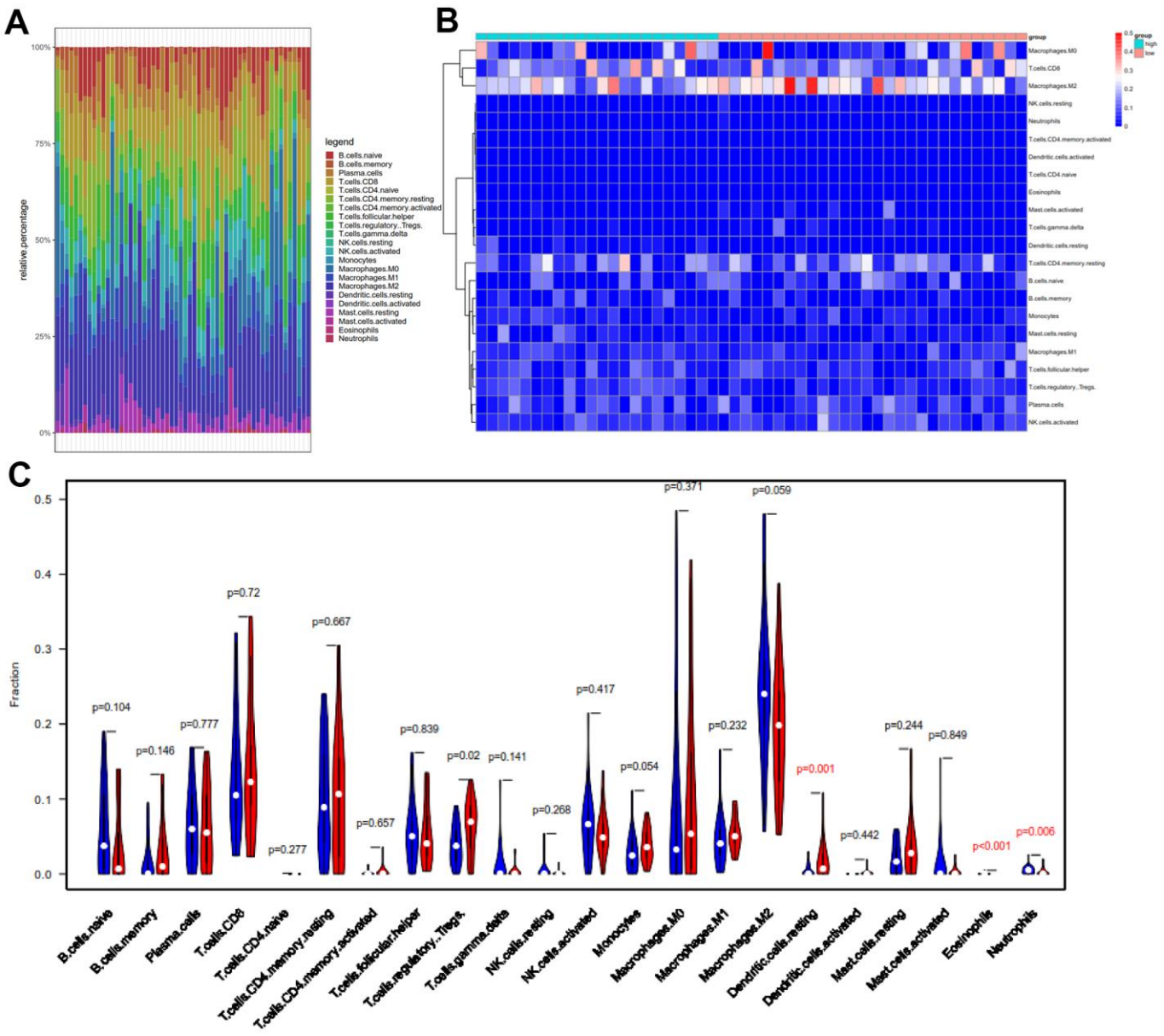

Figure 7. Comparison of 22 important tumor-infiltrating immune Cells (TIICs) between the low-TMB and high-TMB groups. (**A**) Barplot exhibited the proportion of 22 kinds of TIICs in HCC tumor samples, and the different colors represent the 22 TIICs. Vertical and horizontal axes represent relative percentage and patients, respectively. (**B**) Differential abundances of TIICs in the two groups are shown in the heatmap plot. Vertical and horizontal axes represent TIICs and patients, respectively. TIICs with higher and lower correlation levels are shown in red and blue, respectively. Color bars at the top of the heat map represent sample types, with pink and blue indicating low- and high-TMB samples, respectively. (**C**) The violin plot compared the proportions of 22 TIICS between low-TMB and high-TMB groups. Blue and red colors represent low- and high-TMB patients, respectively. Vertical and horizontal axes respectively represent TIICs fraction and TIICs, respectively. The Wilcoxon rank-sum test revealed that the infiltration levels of T cells regulatory (Tregs), dendritic cells resting and eosinophils were higher in the high-TMB group. TMB, tumor mutation burden; TIICs, tumor-infiltrating immune Cells; Tregs, T cells regulatory.

Table 4. Multivariate Cox regression analysis of the immune infiltration cells based on TIMER database in HCC.

Tumor-infiltrating immune cell	Coef	HR	CI95.low	CI95.high	Zscore	P_value
B_cell	–5.334	0.005	0.000	0.787	–2.052	0.040
T_cell_CD4_plus	–3.77	0.023	0.000	2.740	–1.547	0.122
T_cell_CD8_plus	–3.879	0.021	0.001	0.343	–2.705	0.007
Neutrophil	3.561	35.203	0.078	15938.055	1.141	0.254
Macrophage	3.379	29.333	1.567	549.224	2.260	0.024
Dendritic_cell	3.083	21.823	1.927	247.152	2.490	0.013

*Var: Cox univariate analysis immune cells; Coef: Risk coefficient; HR: relative risk value; Ci95.low, CI95.high: range of 95% confidence interval of relative risk value HR; Zscore: Z value of statistical test; P_value: the P value tested by Cox test with one factor. HCC: hepatocellular carcinoma.

accurately predict the 3-year and 5-year survival rate in HCC and BLCA, whether the method maintained the independent predictive value needs to be investigated and validates on larger samples in different cancers.

LGALS3 (Galectin-3) is mainly involved in cell growth, cell adhesion, cell differentiation, and tumor progression and metastasis owing to its action of binding to glycoproteins. Kada found that decreased expression of Galectin-3 in gastric cancer indicated poor prognosis [47]. The core proteoglycan (DCN), a main component of ECM, negatively regulates Tregs [48–52]. DCN can indirectly inhibit the formation of foxp3+ Tregs via the inhibition of the TGF-β signaling pathway [53, 54]. Many studies have demonstrated that DCN overexpression inhibits the progress of various tumors, such as breast cancer and colon cancer [35, 55, 56].

Low expression of FTCD is correlated with poor prognosis ($P < 0.001$) in HCC as per the TCGA data [57]; meanwhile, FTCD overexpression suppressed the proliferation of BEL-7402 and SNU499 cells, resulting in increased PTEN protein and decreased PI3K, total Akt, and phosphorylated Akt protein in BEL-7402 and SNU499 cells. As per a recent study, the PTEN-PI3K/AKT signal transduction pathway was involved in tumor immune escape via the regulation of PD-L1 expression [58]. PD-L1 played an important role in inducing specific T cell apoptosis and tumor immune escape. Thus, FTCD overexpression inhibits tumor progression and tumor immune escape in HCC via the suppression of PI3K/AKT pathway activation. Therefore, FTCD could also be a promising biomarker and a potential target for HCC treatment.

TIMER is the first method for performing integrative analysis of tumor immune cell, clinical, and genomics data [59]. TIMER database was used for assessing the relationships of 9 TMB-related signature with immune infiltration levels in clear cell renal cell carcinoma (ccRCC) [36], the 9 signatures were associated with lower immune infiltrates. After constructing the TMB prognostic model, we also compared the abundance of immune cells utilizing TIMER database, CIBERSORT software, and GSEA database, and found that the prognosis of DCs infiltration was different between high- and low-TMB group. At present, DCs are considered as prognostic indicators in cancers, because the higher infiltrated DCs are associated with better prognosis [60, 61]. Cai et al. found that high infiltration of DC in hepatoma indicates a higher disease-free survival time [60]. Single-cell sequencing of 16,498 HCC cells found that, compared with primary hepatocellular carcinoma, more DCs and CD8+ T cells were infiltrated in early recurrent tumors, while fewer regulatory T cells played an immunosuppressive role [37] in early recurrent tumors. Due to the high affinity of PD-L1 binding to CD80 on the DC surface, CD80 was preferentially bound to PD-L1. Thereby the competitive inhibition that CD80-CD28 mediated CO-stimulation of DC on CD8+ T cells blocked antigen presentation and inhibited the activation of CD8+ T cells. This suggests that the mechanism of immune escape in early recurrent tumors is different from that in primary hepatocellular carcinoma. This will contribute to the development of more effective therapeutic targets and biomarkers for immunotherapy in HCC patients [37]. According to the origin, DCs are divided into DCs derived from myeloid DC (mDC) and lymphatic dendritic cells (LDC) or plasmacytoid dendritic cells (pDC) [62]. In this study, the prognosis of different DC subgroups was different between high-TMB and low-TMB groups. For example, higher fraction of pDCs associated with improved OS rates (Table 5 and Figure 8J) was marginally protective infiltrating cells and immune response in low-TMB group, while higher fraction of pDCs was a hazard risk for high-TMB patients (Table 5). Previous research results shown that Mature pDCs inhibited the tumor, while

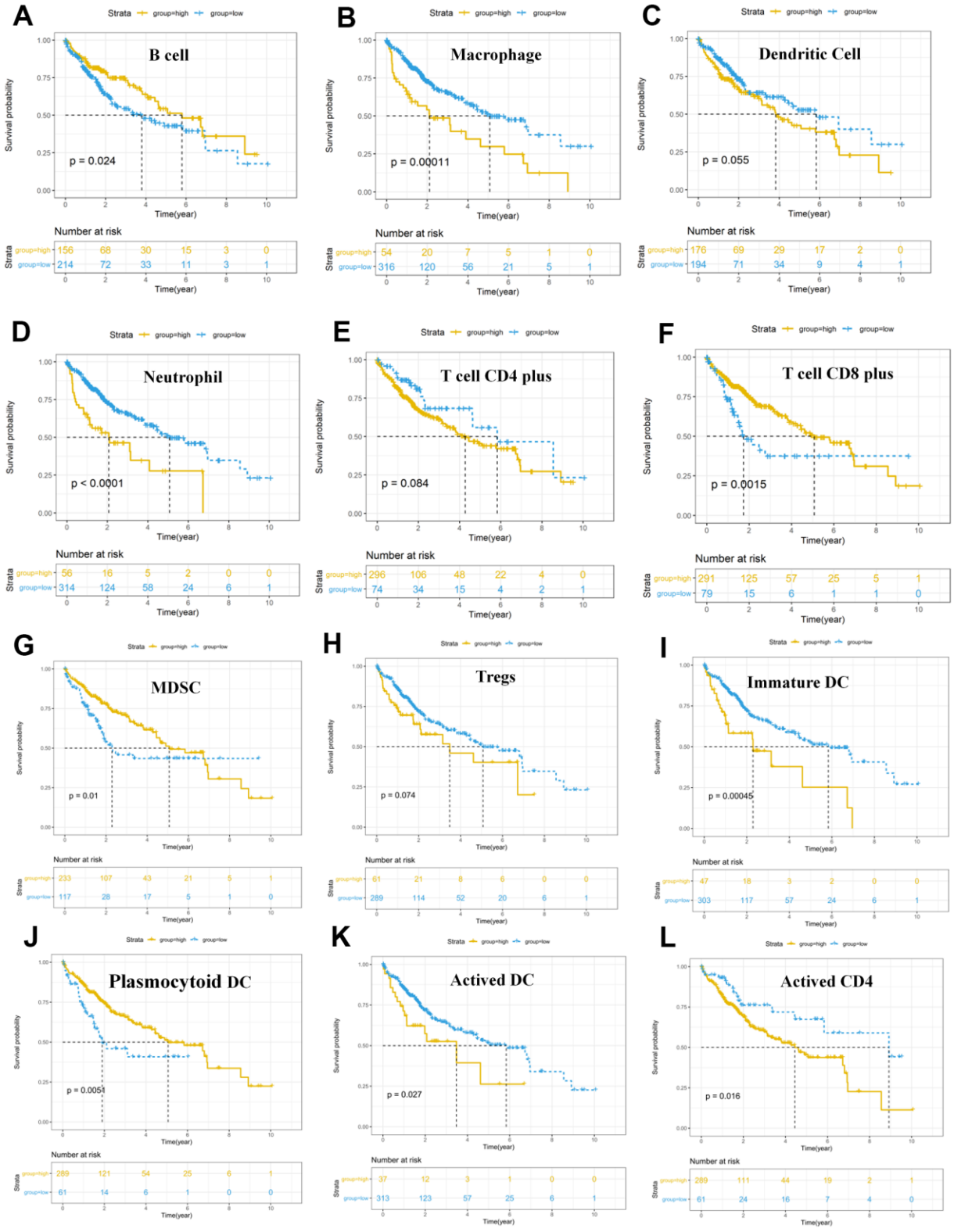

Figure 8. Survival analysis of immune cells based on the TIMER database. Horizontal and vertical axes represent survival times and survival rates, respectively. Yellow and blue curves are samples with higher and lower immune cell fractions, respectively. (**A**–**L**) Lower infiltration levels of macrophages (**B**), dendritic cells (**C**), and neutrophil (**D**), CD4+ T cells (**E**), Tregs (**H**), Immature DC (**I**), Activated DC (**K**) and Activated CD4 (**L**) with improved survival outcomes, and higher infiltration levels of B cells (**A**), CD8+ T cells (**F**), MDSC (**G**) and Plasmocytoid DC (**J**) were associated with poor survival outcomes in HCC. HCC, hepatocellular carcinoma; TIMER, Tumor Immune Estimation Resource; Tregs, T cells regulatory; MDSC, myeloid-derived suppressor cells.

immature pDCs in the tumor microenvironment promoted the tumor [63, 64]. These previous research results might explain that higher infiltration of mature pDCs was favorable factor while immature pDCs was risk factor in HCC. On the other hand, although the fraction of pDCs was not different between the two TMB groups (Figure 9A), pDCs is might mainly mature pDCS in low TMB while immature pDCS in high TMB in HCC. However, this hypothesis needs to be verified by flow cytometry, and/or immunohistochemistry.

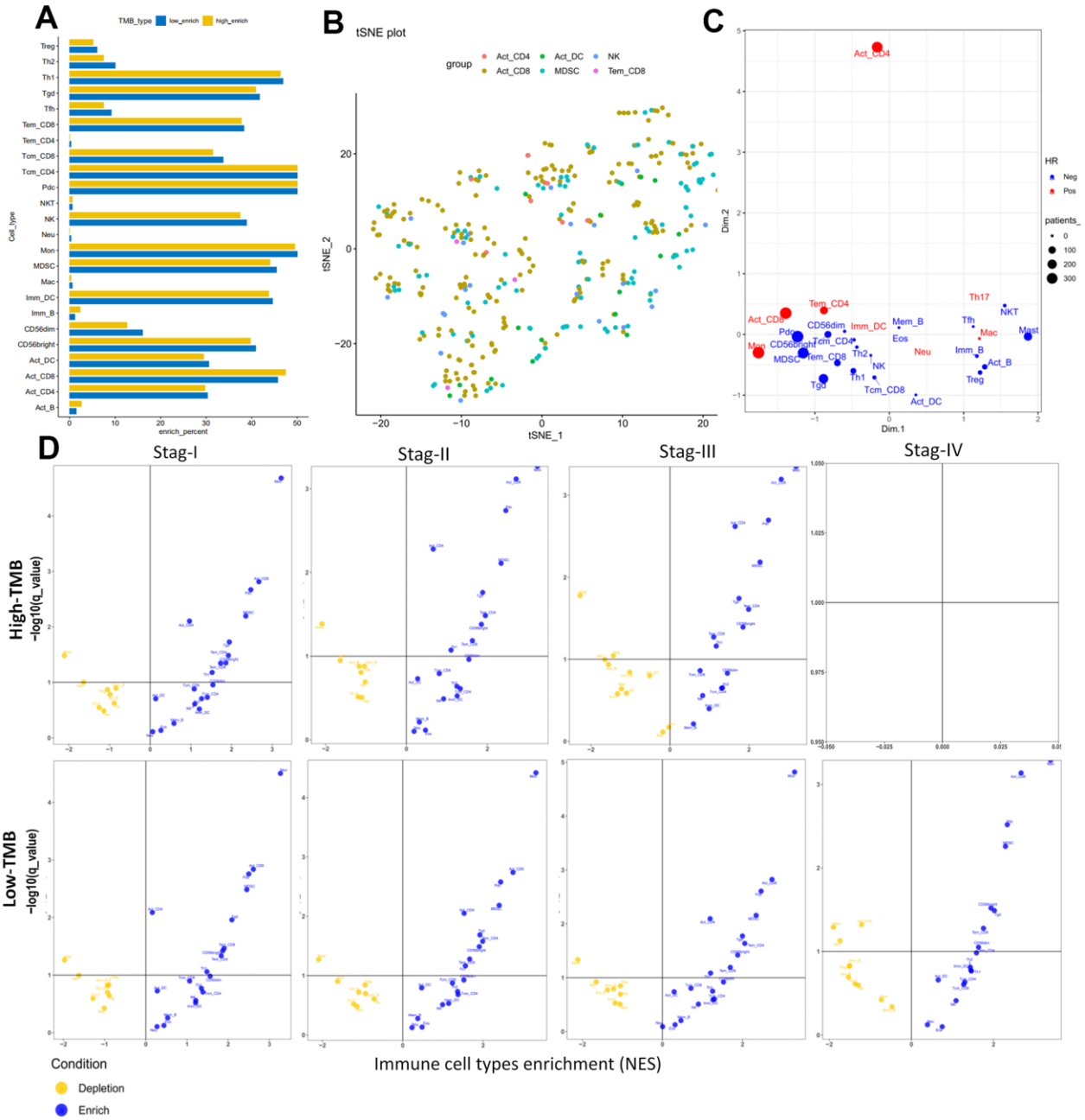

Figure 9. Cellular characterization of immune infiltrates based on GSEA database. (**A**) Correspondence analysis of immune subpopulations in HCC. Horizontal and vertical axes represent enrich percent and immune subpopulations, respectively. Yellow and blue bar are samples with higher and lower immune cell fractions, respectively. (**B**) t-SNE showing individual patients and selected cell types based on two dimensional coordinates. Different colors are different immune subpopulations respectively. (**C**) Visualization of the immune infiltrates for all patients using two dimensional coordinates from multidimensional scaling (MDS). (**D**) Volcano plots for the enrichment (blue) and depletion (yellow) of immune cell types across cancers for tumor stage I to IV calculated based on the NES score in high-TMB (up panel) and low-TMB (down panel) from the GSEA. Horizontal and vertical axes represent Immune cell types enrichment (NES) and −log10(q−value), respectively. There were not any pots in stage IV for high-TMB, because there were not enough samples for analysis.

Table 5. Univariate regression analyses of immune infiltration cells based on GSEA database in HCC.

Tumor-infiltrating immune cell	All samples		High-TMB		low-TMB	
	HR	P.value	HR	P.value	HR	P.value
Act_CD8	2.415	0.002	0.559	0.160	0.621	0.129
Tcm_CD8	0.881	0.085	11.825	0.045	1.138	0.897
Tem_CD8	0.754	0.013	1.465	0.646	0.605	0.478
Act_CD4	1.120	0.008	3.003	0.359	0.864	0.844
Tcm_CD4	0.342	0.011	1.097	0.859	0.774	0.508
Tem_CD4	2.612	0.004	NA	NA	NA	NA
Tfh	0.982	0.842	0.137	0.542	16.591	0.153
Tgd	0.849	0.059	5.022	0.132	1.194	0.818
Th1	0.868	0.073	0.433	0.280	0.623	0.377
Th17	1.015	0.943	NA	NA	NA	NA
Th2	0.911	0.473	0.921	0.984	3.191	0.427
Treg	0.966	0.647	NA	NA	2.241	0.557
Act_B	0.821	0.027	NA	NA	NA	NA
Imm_B	0.903	0.215	NA	NA	NA	NA
Mem_B	0.814	0.044	NA	NA	NA	NA
NK	0.732	0.008	0.527	0.503	0.837	0.784
CD56bright	0.621	0.242	1.012	0.992	1.198	0.839
CD56dim	0.742	0.582	7353.518	0.060	0.471	0.739
MDSC	0.730	0.307	0.942	0.893	1.176	0.668
NKT	0.883	0.720	NA	NA	NA	NA
Act_DC	0.982	0.780	1.291	0.779	2.251	0.210
Pdc	0.576	0.250	1.606	0.428	0.302	0.021
Imm_DC	1.241	0.417	10.151	0.022	2.937	0.151
Mac	1.040	0.778	NA	NA	NA	NA
Eos	0.937	0.597	NA	NA	NA	NA
Mast	0.612	0.032	NA	NA	NA	NA
Mon	1.169	0.635	0.556	0.454	0.836	0.763
Neu	1.029	0.814	NA	NA	NA	NA

HR: relative risk value; P_value: the P value tested by Cox test with multi-factor; NA: The sample size is too small for Cox analysis; HCC: hepatocellular carcinoma, TMB, tumor mutation burden.

In this study, we found that high-TMB patients had higher infiltration levels of resting dendritic cells (DCs) (Figure 7), poor OS (Figure 8), and that higher infiltration levels of mDCs (Table 4), especially the immature DCs (Table 5) was a hazard factor in HCC based on TIMER database and GSEA database. Myeloid-DCs (mDCs) can induce both primary immunosuppression and tumorigenesis [65]. mDCs are considered to be a negative factor in anti-tumor immunity due to their decreased expression and function [66]. Further, in the present study, the infiltration level density of T cells regulatory (Tregs) was higher in the high-TMB group. Previous studies have shown that Tregs could inhibit the proliferation of CD4+ T cells and the secretion of IL-2 [67, 68]. SATO found that the improvement in tumor-specific CD8+ T cells and reduction in Tregs cells can effectively improve the prognosis in cancer patients [69]. Empirical researches have shown that mDCs are related to the selection of thymic Tregs, differentiation, proliferation, and functional regulation of peripheral lymphoid tissues [70, 71].

Although higher macrophage level was a hazard risk factor associated with poor survival outcomes, which is in agreement with that of breast cancer [72], no significantly different macrophage levels were observed in the two TMB groups. Higher MDSCs infiltrations was associated with improved OS, but we couldn't cleanly distinguish the difference of MDSCs infiltrations levels and risk factor of MDSCs between

high-and low -TMB groups in HCC. Therefore, we could not easily determine the potential relationship between TMB, infiltration of macrophage and MDSCs.

In our study, infiltrating levels of DCs, TMB, and TMB-related hub signatures can be used as prognostic indicator in HCC. However, TMB should be analyzed together with DCs infiltrating levels, especially in stage III and stage IV patients, wherein TMB is generally lower. Moreover, the four TMB-related signatures can also be prognosis index in HCC. While there are some limitations should be taken into consideration: (1) although the role of TMB in the prognosis of HCC and its potential relationship with immune cell infiltration had been identified by CIBERSORT software, TIMER database and ssGSEA, different analysis methods also have conflicting conclusions, which need to be verified through a large number of clinical data or clinical trials in the future; (2) The four TMB-related genes and immune cell infiltrates are also needed to be validated based on basic experiment in the future.

CONCLUSIONS

In conclusion, higher TMB correlated with improved survival outcomes and might induce local immune recognition in HCC. Patients were divided in two risk groups using TMBPM based on 4 hub TMB-related signature, and TMBPM index may serve as a promising prognostic biomarker for HCC in the future. Different DC subgroups (mDCS, pDCs and immDCs) and the infiltrating levels of these DC subgroups were different risk factors and also were associated with different survival outcomes between high- and low-TMB samples, while may play an important role in metastasis, suppression and progress of HCC.

MATERIALS AND METHODS

Acquisition of multi-omics data resource

All the data used in this article were obtained from the TCGA database on the GDC website (https://portal.gdc.cancer.gov/), including HCC mutation data; transcriptome profiles; and clinical information, such as age, sex, AJCC-TNM stages, pathological stages, tumor stages, and survival outcomes. The statistical results of somatic mutation were visualized with the maftools software. The transcriptome profiles with HTSeq-FPKM Format of 371 patients were also downloaded from the TCGA database with the GDC tool.

Correlation analysis between TMB and prognosis

First, we filtered out the germline mutations annotated in the dbsnp and ExAC databases. Then, we defined and calculated the TMB of each sample as the total amount of coding variants/the length of exons (38 million), where the detected variants were considered as frameshift deletion mutation, in-frame deletion, frameshift insertion mutation, in-frame insertion, missense mutation, nonsense mutation, nonstop mutation and silent. As per the median TMB value, the patients were divided into the high-TMB and low-TMB groups. Kaplan–Meier survival analysis with log-rank test was performed to assess the differential survival rate between the high-TMB and low-TMB groups. In order to improve the accuracy of Kaplan–Meier survival analysis, we excluded these samples with survival duration of <10 d. Moreover, the association of TMB distribution with several clinical variables (AJCC-TNM stage, tumor stage, and case stage) was evaluated using Kruskal–Wallis test.

Differential expressed genes and functional analysis in the 2 TMB groups

For the high-TMB and low-TMB groups, we used the limma software to identify DEGs in the two groups with $|logFC| > 1.5$ and FDR < 0.05. The heatmap was displayed with the "heatmap" package to visualize the differences. ClusterProfiler package was implemented for GO and KEGG analysis with q value < 0.05. Furthermore, GSEA analysis was performed with FDR < 0.3 based on JAVA8 platform using the TMB level as the phenotype. Moreover, STRINGdb software was used for protein–protein interaction analysis.

Identification of prognostic genes

Thirty TMB-related genes were obtained from 109 DEGs using univariate Cox survival analysis with P < 0.05. Subsequently, four hub TMB-related signatures were identified using the stepwise regression screening method; the process has been shown in the form of a Venn diagram. TMBPM was used to calculate $TMBPM = \Sigma (\beta i \times EXPi)$ based on multivariate Cox analysis. ROC curve was utilized to assess the predictive score of four TMB-related signatures in HCC.

The nomogram of the HCC prognosis model was established via univariate and multivariate analyses, combined with clinical characteristics. Then, calibration curves were constructed for the prediction of 1-year, 3-year, and 5-year survival in HCC.

Assessment of immune-infiltrating cells and prognostic analysis

CIBERSORT software (https://cibersort.stanford.edu) was used to evaluate the compositions of the immune cells in HCC samples, with P > 0.05 to improve accuracy of the estimated results, Heatmap has been

used to show the distribution of immune cell fractions, and violin plot visualizes the differential distributions of cells with two TMB levels.

Based on the TIMER database, multivariate Cox analysis that was fitted by function coxph (β_i) from R package "survival" was used to identify the immune infiltration cells. Subsequently, we calculated the HR with 95% confidence interval (95%CI). Further, Kaplan–Meier survival analysis was performed with a P value < 0.05 of log-rank test to show the differential survival outcomes between different levels of immune infiltrates in HCC.

Subsequently, we identified 28 kinds of immune cells that are over-represented in the tumor microenvironment using single sample gene set enrichment analysis (ssGSEA) [39]. All immune cell types were considered enriched in a patient or group of patients when FDR (q-value) ≤ 0.1 and normalized enrichment score (NES) >0. The similarity of the enrichment of immune infiltrates (averaged NES) were calculated using multidimensional scaling (MDS). The distribution of selected cell types for individual patients were analyzed with t-distributed stochastic neighbor embedding (t-SNE) using the Matlab toolbox t-SNE.

Statistical analyses

All the statistical analyses were conducted using R software (Version 3.5.2). The p-values were adjusted for multiple testing based on FDR according to the Benjamini-Hochberg approach, P value < 0.05 was regarded statistically significant. Differential analysis and normalization were mainly conducted by "limma" package of the R software (version 3.5.2). The Kaplan–Meier analysis with log-rank test or Cox regression model was performed by "survival" package. Student's t test was used for continuous variables, while categorical variables were compared by $\chi 2$ test. The non-parametric two-sided Wilcoxon-rank sum test was utilized for comparing two groups and the Kruskal–Wallis test was suitable when it comes to two or more groups. Differences and correlations among immune cells were analyzed with the vioplot (https://cran.r-project.org/web/packages/vioplot/index.html).

Editorial note

[&]This corresponding author has a verified history of publications using a personal email address for correspondence.

Abbreviations

HCC: hepatocellular carcinoma; GEO: Gene Expression Omnibus; TCGA: The Cancer Genome Atlas; DEGs: differentially expressed genes; TIMER: Tumor Immune Estimation Resource; PPI: protein–protein interaction; GO: Gene Ontology; KEGG: Kyoto Encyclopedia of Genes and Genomes; OS: overall survival; DFI: disease-free interval; TMB: tumor mutation burden; TMBPM: tumor mutation burden prognostic model; ECM: extracellular matrix; TME: tumor microenvironment; DC: dendritic cell; Tregs: T cells regulatory; GSEA: Gene set enrichment analysis; AUC: area under curve; ROC: receiver operating characteristic; ICIs: immune checkpoint inhibitors; ORR: objective response rate; NES: normalized enrichment score; PD-1: programmed death 1 PD-1; PD-L1: programmed death ligand-1; CTLA-4: cytotoxic T-lymphocyte associated antigen-4; DDR: DNA damage repair; ORR: objective response rate; DEL: deletion; INS: insertion; SNV: single nucleotide variants; FDR: false discovery; PPAR: peroxisome proliferators-activated receptor; LGALS3: lectin galactoside-binding soluble 3; NPIPB15: Nuclear Pore Complex Interacting Protein Family Member B15; FTCD: Formimidoyltransferase Cyclodeaminase; DCN: Decorin; MDSCs: myeloid-derived suppressor cells; mDC: myeloid DC; LDC: lymphatic dendritic cells; pDC: plasmacytoid dendritic cells; ccRCC: clear cell renal cell carcinoma; BLCA: bladder cancer.

AUTHOR CONTRIBUTIONS

Shaoqing Liu conceived, designed and write the manuscript. Qianjie Tang and Jianwen Huang collected data, provided bioinformatics analysis and generated the figures and tables. Meixiao Zhan, Wei Zhao, Xiangyu Yang, Yong Li and Lige Qi performed the literature search for the manuscript. Meixiao Zhan, Wei Zhao, Fujun Zhang and Ligong Lu revised the images, the tables and checked the manuscript. Fujun Zhang, Ligong Lu and Xu He directed the manuscript. All authors read and approved the final manuscript.

ACKNOWLEDGMENTS

The authors thank Dr. Lei Xue for editing the manuscript.

CONFLICTS OF INTEREST

The authors declare that they have no conflicts of interest.

FUNDING

This study is supported by the National Key Research and Development Program of China (Grant No. 2017YFA0205200), the National Natural Science Foundation of China (Grant No.81771957, 81901857, 81801811), Natural Science Foundation of Guangdong Province, China (No. 2018A030313074).

REFERENCES

1. Bray F, Ferlay J, Soerjomataram I, Siegel RL, Torre LA, Jemal A. Global cancer statistics 2018: GLOBOCAN estimates of incidence and mortality worldwide for 36 cancers in 185 countries. CA Cancer J Clin. 2018; 68:394–424. https://doi.org/10.3322/caac.21492 PMID:30207593

2. Siegel RL, Miller KD, Jemal A. Cancer statistics, 2015. CA Cancer J Clin. 2015; 65:5–29. https://doi.org/10.3322/caac.21254 PMID:25559415

3. Chen W, Zheng R, Baade PD, Zhang S, Zeng H, Bray F, Jemal A, Yu XQ, He J. Cancer statistics in China, 2015. CA Cancer J Clin. 2016; 66:115–32. https://doi.org/10.3322/caac.21338 PMID:26808342

4. Greten TF, Papendorf F, Bleck JS, Kirchhoff T, Wohlberedt T, Kubicka S, Klempnauer J, Galanski M, Manns MP. Survival rate in patients with hepatocellular carcinoma: a retrospective analysis of 389 patients. Br J Cancer. 2005; 92:1862–68. https://doi.org/10.1038/sj.bjc.6602590 PMID:15870713

5. Bruix J, Reig M, Sherman M. Evidence-based diagnosis, staging, and treatment of patients with hepatocellular carcinoma. Gastroenterology. 2016; 150:835–53. https://doi.org/10.1053/j.gastro.2015.12.041 PMID:26795574

6. Zeng H, Chen W, Zheng R, Zhang S, Ji JS, Zou X, Xia C, Sun K, Yang Z, Li H, Wang N, Han R, Liu S, et al. Changing cancer survival in China during 2003-15: a pooled analysis of 17 population-based cancer registries. Lancet Glob Health. 2018; 6:e555–67. https://doi.org/10.1016/S2214-109X(18)30127-X PMID:29653628

7. Prieto J, Melero I, Sangro B. Immunological landscape and immunotherapy of hepatocellular carcinoma. Nat Rev Gastroenterol Hepatol. 2015; 12:681–700. https://doi.org/10.1038/nrgastro.2015.173 PMID:26484443

8. Sprinzl MF, Galle PR. Current progress in immunotherapy of hepatocellular carcinoma. J Hepatol. 2017; 66:482–84. https://doi.org/10.1016/j.jhep.2016.12.009 PMID:28011330

9. El-Khoueiry AB, Sangro B, Yau T, Crocenzi TS, Kudo M, Hsu C, Kim TY, Choo SP, Trojan J, Welling TH 3rd, Meyer T, Kang YK, Yeo W, et al. Nivolumab in patients with advanced hepatocellular carcinoma (CheckMate 040): an open-label, non-comparative, phase 1/2 dose escalation and expansion trial. Lancet. 2017; 389:2492–502. https://doi.org/10.1016/S0140-6736(17)31046-2 PMID:28434648

10. Zhu AX, Finn RS, Edeline J, Cattan S, Ogasawara S, Palmer D, Verslype C, Zagonel V, Fartoux L, Vogel A, Sarker D, Verset G, Chan SL, et al, and KEYNOTE-224 investigators. Pembrolizumab in patients with advanced hepatocellular carcinoma previously treated with sorafenib (KEYNOTE-224): a non-randomised, open-label phase 2 trial. Lancet Oncol. 2018; 19:940–52. https://doi.org/10.1016/S1470-2045(18)30351-6 PMID:29875066

11. Robert C, Long GV, Brady B, Dutriaux C, Maio M, Mortier L, Hassel JC, Rutkowski P, McNeil C, Kalinka-Warzocha E, Savage KJ, Hernberg MM, Lebbé C, et al. Nivolumab in previously untreated melanoma without BRAF mutation. N Engl J Med. 2015; 372:320–30. https://doi.org/10.1056/NEJMoa1412082 PMID:25399552

12. Herbst RS, Baas P, Kim DW, Felip E, Pérez-Gracia JL, Han JY, Molina J, Kim JH, Arvis CD, Ahn MJ, Majem M, Fidler MJ, de Castro G Jr, et al. Pembrolizumab versus docetaxel for previously treated, PD-L1-positive, advanced non-small-cell lung cancer (KEYNOTE-010): a randomised controlled trial. Lancet. 2016; 387:1540–50. https://doi.org/10.1016/S0140-6736(15)01281-7 PMID:26712084

13. Ansell SM, Lesokhin AM, Borrello I, Halwani A, Scott EC, Gutierrez M, Schuster SJ, Millenson MM, Cattry D, Freeman GJ, Rodig SJ, Chapuy B, Ligon AH, et al. PD-1 blockade with nivolumab in relapsed or refractory Hodgkin's lymphoma. N Engl J Med. 2015; 372:311–19. https://doi.org/10.1056/NEJMoa1411087 PMID:25482239

14. Ferris RL, Blumenschein G Jr, Fayette J, Guigay J, Colevas AD, Licitra L, Harrington K, Kasper S, Vokes EE, Even C, Worden F, Saba NF, Iglesias Docampo LC, et al. Nivolumab for recurrent squamous-cell carcinoma of the head and neck. N Engl J Med. 2016; 375:1856–67. https://doi.org/10.1056/NEJMoa1602252 PMID:27718784

15. Kelderman S, Schumacher TN, Haanen JB. Acquired and intrinsic resistance in cancer immunotherapy. Mol Oncol. 2014; 8:1132–39. https://doi.org/10.1016/j.molonc.2014.07.011 PMID:25106088

16. Mouw KW, Goldberg MS, Konstantinopoulos PA, D'Andrea AD. DNA damage and repair biomarkers of immunotherapy response. Cancer Discov. 2017; 7:675–93.

https://doi.org/10.1158/2159-8290.CD-17-0226
PMID:28630051

17. Le DT, Uram JN, Wang H, Bartlett BR, Kemberling H, Eyring AD, Skora AD, Luber BS, Azad NS, Laheru D, Biedrzycki B, Donehower RC, Zaheer A, et al. PD-1 blockade in tumors with mismatch-repair deficiency. N Engl J Med. 2015; 372:2509–20.
https://doi.org/10.1056/NEJMoa1500596
PMID:26028255

18. Le DT, Durham JN, Smith KN, Wang H, Bartlett BR, Aulakh LK, Lu S, Kemberling H, Wilt C, Luber BS, Wong F, Azad NS, Rucki AA, et al. Mismatch repair deficiency predicts response of solid tumors to PD-1 blockade. Science. 2017; 357:409–13.
https://doi.org/10.1126/science.aan6733
PMID:28596308

19. Chowell D, Morris LG, Grigg CM, Weber JK, Samstein RM, Makarov V, Kuo F, Kendall SM, Requena D, Riaz N, Greenbaum B, Carroll J, Garon E, et al. Patient HLA class I genotype influences cancer response to checkpoint blockade immunotherapy. Science. 2018; 359:582–87.
https://doi.org/10.1126/science.aao4572
PMID:29217585

20. Tran E, Ahmadzadeh M, Lu YC, Gros A, Turcotte S, Robbins PF, Gartner JJ, Zheng Z, Li YF, Ray S, Wunderlich JR, Somerville RP, Rosenberg SA. Immunogenicity of somatic mutations in human gastrointestinal cancers. Science. 2015; 350:1387–90.
https://doi.org/10.1126/science.aad1253
PMID:26516200

21. Strønen E, Toebes M, Kelderman S, van Buuren MM, Yang W, van Rooij N, Donia M, Böschen ML, Lund-Johansen F, Olweus J, Schumacher TN. Targeting of cancer neoantigens with donor-derived T cell receptor repertoires. Science. 2016; 352:1337–41.
https://doi.org/10.1126/science.aaf2288
PMID:27198675

22. Rizvi NA, Hellmann MD, Snyder A, Kvistborg P, Makarov V, Havel JJ, Lee W, Yuan J, Wong P, Ho TS, Miller ML, Rekhtman N, Moreira AL, et al. Cancer immunology. Mutational landscape determines sensitivity to PD-1 blockade in non-small cell lung cancer. Science. 2015; 348:124–28.
https://doi.org/10.1126/science.aaa1348
PMID:25765070

23. Yarchoan M, Hopkins A, Jaffee EM. Tumor mutational burden and response rate to PD-1 inhibition. N Engl J Med. 2017; 377:2500–01.
https://doi.org/10.1056/NEJMc1713444
PMID:29262275

24. McGranahan N, Furness AJ, Rosenthal R, Ramskov S, Lyngaa R, Saini SK, Jamal-Hanjani M, Wilson GA, Birkbak NJ, Hiley CT, Watkins TB, Shafi S, Murugaesu N, et al. Clonal neoantigens elicit T cell immunoreactivity and sensitivity to immune checkpoint blockade. Science. 2016; 351:1463–69.
https://doi.org/10.1126/science.aaf1490
PMID:26940869

25. Hellmann MD, Ciuleanu TE, Pluzanski A, Lee JS, Otterson GA, Audigier-Valette C, Minenza E, Linardou H, Burgers S, Salman P, Borghaei H, Ramalingam SS, Brahmer J, et al. Nivolumab plus ipilimumab in lung cancer with a high tumor mutational burden. N Engl J Med. 2018; 378:2093–104.
https://doi.org/10.1056/NEJMoa1801946
PMID:29658845

26. Sahin U, Derhovanessian E, Miller M, Kloke BP, Simon P, Löwer M, Bukur V, Tadmor AD, Luxemburger U, Schrörs B, Omokoko T, Vormehr M, Albrecht C, et al. Personalized RNA mutanome vaccines mobilize poly-specific therapeutic immunity against cancer. Nature. 2017; 547:222–26.
https://doi.org/10.1038/nature23003 PMID:28678784

27. Miura Y, Sunaga N. Role of immunotherapy for oncogene-driven non-small cell lung cancer. Cancers (Basel). 2018; 10:245.
https://doi.org/10.3390/cancers10080245
PMID:30060457

28. Gainor JF, Shaw AT, Sequist LV, Fu X, Azzoli CG, Piotrowska Z, Huynh TG, Zhao L, Fulton L, Schultz KR, Howe E, Farago AF, Sullivan RJ, et al. EGFR mutations and ALK rearrangements are associated with low response rates to PD-1 pathway blockade in non-small cell lung cancer: a retrospective analysis. Clin Cancer Res. 2016; 22:4585–93.
https://doi.org/10.1158/1078-0432.CCR-15-3101
PMID:27225694

29. Garassino MC, Cho BC, Kim JH, Mazières J, Vansteenkiste J, Lena H, Corral Jaime J, Gray JE, Powderly J, Chouaid C, Bidoli P, Wheatley-Price P, Park K, et al, and ATLANTIC Investigators. Durvalumab as third-line or later treatment for advanced non-small-cell lung cancer (ATLANTIC): an open-label, single-arm, phase 2 study. Lancet Oncol. 2018; 19:521–36.
https://doi.org/10.1016/S1470-2045(18)30144-X
PMID:29545095

30. Shin DS, Zaretsky JM, Escuin-Ordinas H, Garcia-Diaz A, Hu-Lieskovan S, Kalbasi A, Grasso CS, Hugo W, Sandoval S, Torrejon DY, Palaskas N, Rodriguez GA, Parisi G, et al. Primary resistance to PD-1 blockade mediated by JAK1/2 mutations. Cancer Discov. 2017; 7:188–201.
https://doi.org/10.1158/2159-8290.CD-16-1223
PMID:27903500

31. Ruffini E, Asioli S, Filosso PL, Lyberis P, Bruna MC, Macrì

L, Daniele L, Oliaro A. Clinical significance of tumor-infiltrating lymphocytes in lung neoplasms. Ann Thorac Surg. 2009; 87:365–71. https://doi.org/10.1016/j.athoracsur.2008.10.067 PMID:19161739

32. Fridman WH, Zitvogel L, Sautès-Fridman C, Kroemer G. The immune contexture in cancer prognosis and treatment. Nat Rev Clin Oncol. 2017; 14:717–34. https://doi.org/10.1038/nrclinonc.2017.101 PMID:28741618

33. Zhang C, Shen L, Qi F, Wang J, Luo J. Multi-omics analysis of tumor mutation burden combined with immune infiltrates in bladder urothelial carcinoma. J Cell Physiol. 2020; 235:3849–63. https://doi.org/10.1002/jcp.29279 PMID:31596511

34. Wang X, Li M. Correlate tumor mutation burden with immune signatures in human cancers. BMC Immunol. 2019; 20:4. https://doi.org/10.1186/s12865-018-0285-5 PMID:30634925

35. Chen J, Chen Z, Huang Z, Yu H, Li Y, Huang W. Formiminotransferase cyclodeaminase suppresses hepatocellular carcinoma by modulating cell apoptosis, DNA damage, and phosphatidylinositol 3-kinases (PI3K)/Akt signaling pathway. Med Sci Monit. 2019; 25:4474–84. https://doi.org/10.12659/MSM.916202 PMID:31203308

36. Zhang C, Li Z, Qi F, Hu X, Luo J. Exploration of the relationships between tumor mutation burden with immune infiltrates in clear cell renal cell carcinoma. Ann Transl Med. 2019; 7:648. https://doi.org/10.21037/atm.2019.10.84 PMID:31930049

37. Sun Y, Wu L, Zhong Y, Zhou K, Hou Y, Wang Z, Zhang Z, Xie J, Wang C, Chen D, Huang Y, Wei X, Shi Y, et al. Single-cell landscape of the ecosystem in early-relapse hepatocellular carcinoma. Cell. 2021; 184:404–21.e16. https://doi.org/10.1016/j.cell.2020.11.041 PMID:33357445

38. Azizi E, Carr AJ, Plitas G, Cornish AE, Konopacki C, Prabhakaran S, Nainys J, Wu K, Kiseliovas V, Setty M, Choi K, Fromme RM, Dao P, et al. Single-cell map of diverse immune phenotypes in the breast tumor microenvironment. Cell. 2018; 174:1293–308.e36. https://doi.org/10.1016/j.cell.2018.05.060 PMID:29961579

39. Charoentong P, Finotello F, Angelova M, Mayer C, Efremova M, Rieder D, Hackl H, Trajanoski Z. Pan-cancer immunogenomic analyses reveal genotype-immunophenotype relationships and predictors of response to checkpoint blockade. Cell Rep. 2017; 18:248–62. https://doi.org/10.1016/j.celrep.2016.12.019 PMID:28052254

40. Wang L, Yan K, Zhou J, Zhang N, Wang M, Song J, Zhao J, Zhang Y, Cai S, Wang L. Relationship of liver cancer with LRP1B or TP53 mutation and tumor mutation burden and survival. J Clin Oncol. 2019; 37:1573. https://doi.org/10.1200/JCO.2019.37.15_suppl.1573

41. Li L, Rao X, Wen Z, Ding X, Wang X, Xu W, Meng C, Yi Y, Guan Y, Chen Y, Wang J, Jun L. Implications of driver genes associated with a high tumor mutation burden identified using next-generation sequencing on immunotherapy in hepatocellular carcinoma. Oncol Lett. 2020; 19:2739–48. https://doi.org/10.3892/ol.2020.11372 PMID:32218826

42. Lee CK, Man J, Lord S, Links M, Gebski V, Mok T, Yang JC. Checkpoint inhibitors in metastatic EGFR-mutated non-small cell lung cancer-a meta-analysis. J Thorac Oncol. 2017; 12:403–07. https://doi.org/10.1016/j.jtho.2016.10.007 PMID:27765535

43. Spigel DR, Schrock AB, Fabrizio D, Frampton GM, Sun J, He J, Gowen K, Johnson ML, Bauer TM, Kalemkerian GP, Raez LE, Ou SHI, Ross JS, et al. Total mutation burden (TMB) in lung cancer (LC) and relationship with response to PD-1/PD-L1 target therapies. J Clin Oncol. 2016; 34:9017. https://doi.org/10.1200/JCO.2016.34.15_suppl.9017

44. Park SE, Park K, Lee E, Kim JY, Ahn JS, Im YH, Lee C, Jung H, Cho SY, Park WY, Cristescu R, Park YH. Clinical implication of tumor mutational burden in patients with HER2-positive refractory metastatic breast cancer. Oncoimmunology. 2018; 7:e1466768. https://doi.org/10.1080/2162402X.2018.1466768 PMID:30221068

45. Samstein RM, Lee CH, Shoushtari AN, Hellmann MD, Shen R, Janjigian YY, Barron DA, Zehir A, Jordan EJ, Omuro A, Kaley TJ, Kendall SM, Motzer RJ, et al. Tumor mutational load predicts survival after immunotherapy across multiple cancer types. Nat Genet. 2019; 51:202–06. https://doi.org/10.1038/s41588-018-0312-8 PMID:30643254

46. Goodman AM, Kato S, Bazhenova L, Patel SP, Frampton GM, Miller V, Stephens PJ, Daniels GA, Kurzrock R. Tumor Mutational Burden as an Independent Predictor of Response to Immunotherapy in Diverse Cancers. Mol Cancer Ther. 2017; 16:2598–608. https://doi.org/10.1158/1535-7163.MCT-17-0386

PMID:28835386

47. Okada K, Shimura T, Suehiro T, Mochiki E, Kuwano H. Reduced galectin-3 expression is an indicator of unfavorable prognosis in gastric cancer. Anticancer Res. 2006; 26:1369–76. PMID:16619546

48. Yoon AR, Hong J, Yun CO. Adenovirus-mediated decorin expression induces cancer cell death through activation of p53 and mitochondrial apoptosis. Oncotarget. 2017; 8:76666–85. https://doi.org/10.18632/oncotarget.20800 PMID:29100340

49. Goldoni S, Iozzo RV. Tumor microenvironment: modulation by decorin and related molecules harboring leucine-rich tandem motifs. Int J Cancer. 2008; 123:2473–79. https://doi.org/10.1002/ijc.23930 PMID:18798267

50. Sofeu Feugaing DD, Götte M, Viola M. More than matrix: the multifaceted role of decorin in cancer. Eur J Cell Biol. 2013; 92:1–11. https://doi.org/10.1016/j.ejcb.2012.08.004 PMID:23058688

51. Hildebrand A, Romarís M, Rasmussen LM, Heinegård D, Twardzik DR, Border WA, Ruoslahti E. Interaction of the small interstitial proteoglycans biglycan, decorin and fibromodulin with transforming growth factor beta. Biochem J. 1994; 302:527–34. https://doi.org/10.1042/bj3020527 PMID:8093006

52. Iozzo RV, Buraschi S, Genua M, Xu SQ, Solomides CC, Peiper SC, Gomella LG, Owens RC, Morrione A. Decorin antagonizes IGF receptor I (IGF-IR) function by interfering with IGF-IR activity and attenuating downstream signaling. J Biol Chem. 2011; 286:34712–21. https://doi.org/10.1074/jbc.M111.262766 PMID:21840990

53. Konkel JE, Jin W, Abbatiello B, Grainger JR, Chen W. Thymocyte apoptosis drives the intrathymic generation of regulatory T cells. Proc Natl Acad Sci USA. 2014; 111:E465–73. https://doi.org/10.1073/pnas.1320319111 PMID:24474796

54. Carambia A, Freund B, Schwinge D, Heine M, Laschtowitz A, Huber S, Wraith DC, Korn T, Schramm C, Lohse AW, Heeren J, Herkel J. TGF-β-dependent induction of $CD4^+CD25^+Foxp3^+$ Tregs by liver sinusoidal endothelial cells. J Hepatol. 2014; 61:594–99. https://doi.org/10.1016/j.jhep.2014.04.027 PMID:24798620

55. Gubbiotti MA, Vallet SD, Ricard-Blum S, Iozzo RV. Decorin interacting network: a comprehensive analysis of decorin-binding partners and their versatile functions. Matrix Biol. 2016; 55:7–21. https://doi.org/10.1016/j.matbio.2016.09.009 PMID:27693454

56. Nyman MC, Sainio AO, Pennanen MM, Lund RJ, Vuorikoski S, Sundström JT, Järveläinen HT. Decorin in human colon cancer: localization *in vivo* and effect on cancer cell behavior *in vitro*. J Histochem Cytochem. 2015; 63:710–20. https://doi.org/10.1369/0022155415590830 PMID:26001829

57. Bozoky B, Savchenko A, Guven H, Ponten F, Klein G, Szekely L. Decreased decorin expression in the tumor microenvironment. Cancer Med. 2014; 3:485–91. https://doi.org/10.1002/cam4.231 PMID:24634138

58. Parsa AT, Waldron JS, Panner A, Crane CA, Parney IF, Barry JJ, Cachola KE, Murray JC, Tihan T, Jensen MC, Mischel PS, Stokoe D, Pieper RO. Loss of tumor suppressor PTEN function increases B7-H1 expression and immunoresistance in glioma. Nat Med. 2007; 13:84–88. https://doi.org/10.1038/nm1517 PMID:17159987

59. Li T, Fan J, Wang B, Traugh N, Chen Q, Liu JS, Li B, Liu XS. TIMER: a web server for comprehensive analysis of tumor-infiltrating immune cells. Cancer Res. 2017; 77:e108–10. https://doi.org/10.1158/0008-5472.CAN-17-0307 PMID:29092952

60. Cai XY, Gao Q, Qiu SJ, Ye SL, Wu ZQ, Fan J, Tang ZY. Dendritic cell infiltration and prognosis of human hepatocellular carcinoma. J Cancer Res Clin Oncol. 2006; 132:293–301. https://doi.org/10.1007/s00432-006-0075-y PMID:16421755

61. Inoshima N, Nakanishi Y, Minami T, Izumi M, Takayama K, Yoshino I, Hara N. The influence of dendritic cell infiltration and vascular endothelial growth factor expression on the prognosis of non-small cell lung cancer. Clin Cancer Res. 2002; 8:3480–86. PMID:12429638

62. Eisenbarth SC. Dendritic cell subsets in T cell programming: location dictates function. Nat Rev Immunol. 2019; 19:89–103. https://doi.org/10.1038/s41577-018-0088-1 PMID:30464294

63. Salio M, Cella M, Vermi W, Facchetti F, Palmowski MJ, Smith CL, Shepherd D, Colonna M, Cerundolo V. Plasmacytoid dendritic cells prime IFN-gamma-secreting melanoma-specific CD8 lymphocytes and are found in primary melanoma lesions. Eur J Immunol. 2003; 33:1052–62.

https://doi.org/10.1002/eji.200323676
PMID:12672071

64. Le Mercier I, Poujol D, Sanlaville A, Sisirak V, Gobert M, Durand I, Dubois B, Treilleux I, Marvel J, Vlach J, Blay JY, Bendriss-Vermare N, Caux C, et al. Tumor promotion by intratumoral plasmacytoid dendritic cells is reversed by TLR7 ligand treatment. Cancer Res. 2013; 73:4629–40.
https://doi.org/10.1158/0008-5472.CAN-12-3058
PMID:23722543

65. Bracamonte-Baran W, Florentin J, Zhou Y, Jankowska-Gan E, Haynes WJ, Zhong W, Brennan TV, Dutta P, Claas FH, van Rood JJ, Burlingham WJ. Modification of host dendritic cells by microchimerism-derived extracellular vesicles generates split tolerance. Proc Natl Acad Sci USA. 2017; 114:1099–104.
https://doi.org/10.1073/pnas.1618364114
PMID:28096390

66. Lohela M, Casbon AJ, Olow A, Bonham L, Branstetter D, Weng N, Smith J, Werb Z. Intravital imaging reveals distinct responses of depleting dynamic tumor-associated macrophage and dendritic cell subpopulations. Proc Natl Acad Sci USA. 2014; 111:E5086–95.
https://doi.org/10.1073/pnas.1419899111
PMID:25385645

67. Yu A, Snowhite I, Vendrame F, Rosenzwajg M, Klatzmann D, Pugliese A, Malek TR. Selective IL-2 responsiveness of regulatory T cells through multiple intrinsic mechanisms supports the use of low-dose IL-2 therapy in type 1 diabetes. Diabetes. 2015; 64:2172–83.
https://doi.org/10.2337/db14-1322 PMID:25576057

68. Shi C, Zhang Y, Yang H, Dong T, Chen Y, Xu Y, Yang X, Liu P. Ultrasound-targeted microbubble destruction-mediated Foxp3 knockdown may suppress the tumor growth of HCC mice by relieving immunosuppressive Tregs function. Exp Ther Med. 2018; 15:31–38.
https://doi.org/10.3892/etm.2017.5421
PMID:29387180

69. Sato E, Olson SH, Ahn J, Bundy B, Nishikawa H, Qian F, Jungbluth AA, Frosina D, Gnjatic S, Ambrosone C, Kepner J, Odunsi T, Ritter G, et al. Intraepithelial CD8+ tumor-infiltrating lymphocytes and a high CD8+/regulatory T cell ratio are associated with favorable prognosis in ovarian cancer. Proc Natl Acad Sci USA. 2005; 102:18538–43.
https://doi.org/10.1073/pnas.0509182102
PMID:16344461

70. Tarbell KV, Petit L, Zuo X, Toy P, Luo X, Mqadmi A, Yang H, Suthanthiran M, Mojsov S, Steinman RM. Dendritic cell-expanded, islet-specific CD4+ CD25+ CD62L+ regulatory T cells restore normoglycemia in diabetic NOD mice. J Exp Med. 2007; 204:191–201.
https://doi.org/10.1084/jem.20061631
PMID:17210729

71. Liu YJ. A unified theory of central tolerance in the thymus. Trends Immunol. 2006; 27:215–21.
https://doi.org/10.1016/j.it.2006.03.004
PMID:16580260

72. Heys SD, Stewart KN, McKenzie EJ, Miller ID, Wong SY, Sellar G, Rees AJ. Characterisation of tumour-infiltrating macrophages: impact on response and survival in patients receiving primary chemotherapy for breast cancer. Breast Cancer Res Treat. 2012; 135:539–48.
https://doi.org/10.1007/s10549-012-2190-6
PMID:22886449

SUPPLEMENTARY MATERIALS

Supplementary Tables

Please browse Full Text version to see the data of Supplementary Tables 1–4.

Supplementary Table 1. Calculation of tumor mutation burden (TMB) for 363 HCC patients.

Supplementary Table 2. Analysis of differentially expressed genes between the two tumor mutation burden (TMB) groups.

Supplementary Table 3. Top gene ontology (GO) items for differentially expressed genes.

Supplementary Table 4. Univariate cox survival analysis of the differentially expressed genes.